Werk

Jahr: 1985
Kollektion: fid.geo
Signatur: 8 Z NAT 2148:58
Digitalisiert: Niedersächsische Staats- und Universitätsbibliothek Göttingen
Werk Id: PPN1015067948_0058
PURL: http://resolver.sub.uni-goettingen.de/purl?PPN1015067948_0058

LOG Id: LOG_0022
LOG Titel: Numerical experiment in seismic investigations
LOG Typ: article

Übergeordnetes Werk

Werk Id: PPN1015067948
PURL: http://resolver.sub.uni-goettingen.de/purl?PPN1015067948
OPAC: http://opac.sub.uni-goettingen.de/DB=1/PPN?PPN=1015067948

Contact

Niedersächsische Staats- und Universitätsbibliothek Göttingen
Georg-August-Universität Göttingen
Platz der Göttinger Sieben 1
37073 Göttingen
Germany
Email: gdz@sub.uni-goettingen.de

J Geophys (1985) 58:101-124

Journal of Geophysics

Numerical experiment in seismic investigations

B.G. Mikhailenko

Computing center, USSR Academy of Sciences, Siberian Division, Prospekt akademika Lavrentieva, 6, 630090, Novosibirsk, USSR

Abstract. Four stages of numerical experiment in seismology and seismic prospecting are considered. These stages are discussed for different models of a medium. Anisotropic, porous and nonelastic media, whose parameters are arbitrary functions of the vertical coordinate, and 2-D-inhomogeneous elastic media, whose parameters are arbitrary functions of two coordinates, are dealt with. For solving these problems, different algorithms are suggested which are based on a combination of finite integral transforms with finite-difference techniques. Complete theoretical seismograms for anisotropic, porous and nonelastic media and for complex 3-D-geometries are presented.

Of special importance is the analysis of theoretical seismograms for *SH* waves and *P-SV* waves for complex subsurface geometries. From the calculations it is concluded that diffracted-reflected waves can be rather intense, and that they may be used in seismic exploration. A corresponding approach is proposed which implies cancellation of multiple waves and investigation of diffracted waves.

Key words: Elastic wave propagation - Theoretical seismograms - Finite differences - Finite integral transforms

1. Introduction

In this lecture, we will consider some problems and results of numerical seismic modelling for complex geological media. Recently, at the beginning of the 1960s, in seismology and seismic prospecting a new theoretical approach has appeared, which is the numerical experiment. With the help of numerical experiments it became possible to calculate complete theoretical seismograms and to compare them to observed records. In a numerical experiment one can distinguish several stages. First of all, we will briefly characterize each stage and then illustrate all the stages in more detail by particular examples.

Stage 1. Construction of a physical model of a realistic medium.

This stage requires a good knowledge of experimental facts. With the accumulation of experimental data our views change. For example, by the end of the 1950s, in interpreting seismic data of deep seismic sounding a model of the Earth's crust was considered to be made up of thick, homogeneous layers. Then inhomogeneous layers were introduced in the model. After that, a model with lateral inhomogeneities and curved interfaces was developed. Thus, the accumulating data brought out a more flexible physical model than a one-dimensional model. We are now in a transition period from the 1-D model to the 3-D model.

Stage 2. Construction of a mathematical model of a realistic medium.

Now, a physical model selected at stage 1 must be formulated in terms of mathematics. In seismology, a linear-elastic model of a medium is widely used. This model is described by the elastodynamic equations with variable coefficients. For calculated theoretical seismograms to be in good agreement with observed records, it is necessary to develop a mathematical model which takes into account many physical effects. To describe seismic processes in realistic media mathematical models of nonelastic, anisotropic and porous media must be considered. A good selection of a mathematical model makes it possible not only to explain well-known seismic phenomena, but also to predict some new physical effects.

Stage 3. The development of an efficient algorithm for the selected mathematical model of a realistic medium.

The main feature of this stage is the selection of the technique for the calculation of complete theoretical seismograms for the mathematical model of the medium. At present there exist many methods of calculation of theoretical seismograms. Each one of the methods has a corresponding set of problems for which it is best suited. Most of these methods, however, cannot be used for general laterally inhomogeneous media with curved interfaces. There are several approaches at present for the computation of theoretical seismograms for elastic waves in media where the elastic parameters are functions of two coordinates. Only two approaches will be mentioned here.

The first approach is based on the direct numerical solution of the elastodynamic equations by means of finite difference or finite elements techniques. The second approach amploys approximate methods such as asymptotic ray theory and its various modifications and combinations with other methods.

Here we will discuss the method for calculation of complete theoretical seismograms for arbitrary subsurface geometries, based on the combination of finite-integral transforms and finite-difference techniques.

Stage 4. The comparison of theoretical and experimental seismograms.

At this stage, we compare complete theoretical and experimental seismograms and make conclusions about the suitability of our physical model. If the results of this comparison are not satisfactory, we must return to the first stage and change the physical model of a medium and then repeat the whole cycle of the numerical experiment.

Let us illustrate these four stages of the numerical experiment on some particular examples. As physical models of realistic media we will consider the following:

anisotropic model,
porous model,
nonelastic model (Boltzmann's model) and
elastic 2-D inhomogeneous model.

For all these models we will show efficient numerical algorithms for calculating complete theoretical seismograms. All these algorithms are based on the idea of combination of finite-integral transforms with finite-difference techniques.

2. Computation of complete theoretical seismograms for transversely isotropic media

The need to include anisotropy in the description of Earth models was recognized early in the development of seismic investigations. The review of theoretical and experimental results can be found, for example, in papers by Crampin (1981) and White (1982). Here we will discuss the case of a transversely isotropic medium with the axis of symmetry perpendicular to the laminations. Thus, we have fixed a physical model.

Seismic wave propagation in such a medium is described in the cylindrical system of coordinates (r, z) by equations of the form

$$\begin{aligned}\rho\frac{\partial^2 U_r}{\partial t^2}&=c_{11}\left(\frac{\partial^2 U_r}{\partial r^2}+\frac{1}{r}\frac{\partial U_r}{\partial r}-\frac{U_r}{r^2}\right)\\&\quad+c_{13}\frac{\partial^2 U_z}{\partial z\,\partial r}+\frac{\partial}{\partial z}\left[c_{44}\left(\frac{\partial U_r}{\partial z}+\frac{\partial U_z}{\partial r}\right)\right]+\rho F_r,\\\rho\frac{\partial^2 U_z}{\partial t^2}&=c_{44}\left[\frac{\partial}{\partial r}\left(\frac{\partial U_r}{\partial r}+\frac{\partial U_z}{\partial r}\right)+\frac{1}{r}\left(\frac{\partial U_r}{\partial z}+\frac{\partial U_z}{\partial r}\right)\right]\\&\quad+\frac{\partial}{\partial z}\left[c_{13}\left(\frac{\partial U_r}{\partial r}+\frac{U_r}{r}\right)+c_{33}\frac{\partial U_z}{\partial z}\right]+\rho F_z.\end{aligned}\tag{1}$$

Here, the coefficients $c_{ij}(z)$ and the density $\rho(z)$ are arbitrary functions of the variable $z\cdot F_r$ and F_z are components of the excitation vector. For an explosive-type source:

$$\begin{aligned}F_r&=\frac{d}{dr}\left[\frac{\delta(r)}{2\pi r}\right]\delta(z-d)\,f(t),\\F_z&=\frac{\delta(r)}{2\pi r}\frac{d}{dz}[\delta(z-d)]\,f(t).\end{aligned}\tag{2}$$

Here d is the depth of the source and $f(t)$ represents the time variation of the source. At the free surface the boundary conditions of the form

$$\sigma_z|_{z=0}=\left[c_{13}\left(\frac{\partial U_r}{\partial r}-\frac{U_z}{r}\right)+c_{44}\frac{\partial U_z}{\partial z}\right]=0,\tag{3}$$

$$\tau_{rz}|_{z=0}=c_{44}\left(\frac{\partial U_r}{\partial z}-\frac{\partial U_z}{\partial r}\right)=0\tag{4}$$

are fulfilled.

This problem is solved with zero initial data

$$U_r|_{t=0}=U_z|_{t=0}=\left.\frac{\partial U_r}{\partial t}\right|_{t=0}=\left.\frac{\partial U_z}{\partial t}\right|_{t=0}=0.\tag{5}$$

According to the third stage of the computational experiment it is necessary to select a method to calculate the complete theoretical seismograms for an anisotropic medium. Here we make use of the method based on a combination of partial separation of variables and finite-difference techniques. For the inhomogeneous isotropic medium this method was developed in a number of papers (see, for example, Mikhailenko, 1973; Alekseev and Mikhailenko, 1976, 1978, 1980). This approach has been extended to inhomogeneous anisotropic media by Martynov and Mikhailenko (1979, 1984). Following these papers for the solution of problem (1)–(5) we apply as a first step finite Hankel integral transformations of the form

$$R(z,k_i,t)=\int_0^a r\,U_z(z,r,t)\,J_0(k_i r)\,dr,\tag{6}$$

$$U_z(z,r,t)=\frac{2}{a^2}\sum_{i=1}^{\infty}R(z,k_i,t)\frac{J_0(k_i r)}{[J_0(k_i a)]^2},\tag{7}$$

$$S(z,k_i,t)=\int_0^a r\,U_r(z,r,t)\,J_1(k_i r)\,dr,\tag{8}$$

$$U_r(z,r,t)=\frac{2}{a^2}\sum_{i=1}^{\infty}S(z,k_i,t)\frac{J_1(k_i r)}{[J_2(k_i a)]^2},\tag{9}$$

where k_i are the roots of the equation $J_1(k_i a)=0$.

At the boundary $r=a$ we introduce the additional boundary conditions:

$$U_r|_{r=a}=\left.\frac{\partial U_z}{\partial r}\right|_{r=a}=0.\tag{10}$$

In order to exclude wave reflections from this boundary, we select a distance $r=a$ which is large enough.

Employing the finite integral Hankel transform we then obtain the following set of equations:

$$\rho\frac{\partial^2 S}{\partial t^2}=\frac{\partial}{\partial z}\left(c_{44}\frac{\partial S}{\partial z}-k_i c_{44}R\right)-k_i c_{13}\frac{\partial R}{\partial z}-k_i^2 c_{11}S+\rho\hat{F}_r,\tag{11}$$

$$\rho\frac{\partial^2 R}{\partial t^2}=\frac{\partial}{\partial z}\left(c_{33}\frac{\partial R}{\partial z}+k_i c_{13}S\right)+k_i c_{44}\frac{\partial S}{\partial z}-k_i^2 c_{44}R+\rho\hat{F}_z,\tag{12}$$

$$\left[c_{44}\left(\frac{\partial S}{\partial z}-k_i R\right)\right]\Big|_{z=0}=0,\qquad\left(c_{33}\frac{\partial R}{\partial z}+k_i c_{13}S\right)\Big|_{z=0}=0,\tag{13}$$

$$S(z,k_i,t)|_{t=0}=R(z,k_i,t)|_{t=0}=\left.\frac{\partial S}{\partial t}\right|_{t=0}=\left.\frac{\partial R}{\partial t}\right|_{t=0}=0, \qquad (14)$$

where

$$\hat{F}_r=-\frac{1}{2\pi}\delta(z-d)\,f(t)\,k_i,$$
$$\hat{F}_z=\frac{1}{2\pi}\frac{d}{dz}[\delta(z-d)]\,f(t). \qquad (15)$$

We solve the system of Eqs. (11)–(14) by the finite difference method. Here we use an explicit finite-difference scheme in the space of grid variables $z_m=m\Delta z$, $t_j=j\cdot\Delta t$ with truncation errors of second approximation order.

We must solve problem (11)–(14) for different fixed values of k_i, the roots of Bessel equation, and then sum up the series (7) and (9) in order to obtain displacement components.

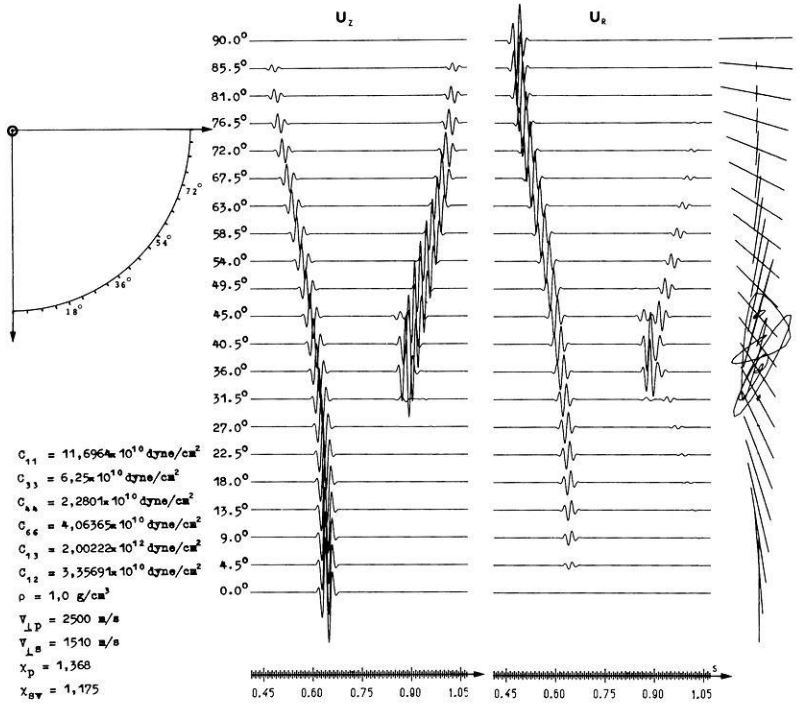

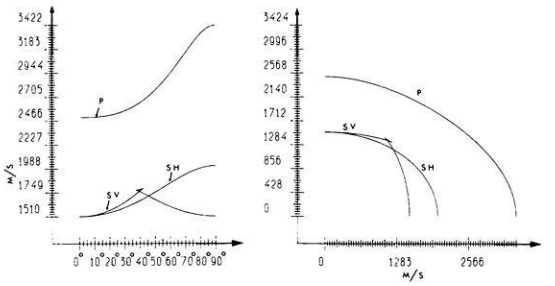

Fig. 1. Theoretical seismograms of the vertical U_z and the horizontal U_R components and parameters of a transversely isotropic model medium. The seismograms are calculated along the radius $R=0.65$ km. Here $\chi_P=V_{P\|}/V_{P\perp}$, $\chi_{SV}=V_{S_{max}}/V_{S\perp}$. $\chi_P=V_{P\|}/V_{P\perp}$, $\chi_{SV}=V_{S_{max}}/V_{S\perp}$. The dominant frequency of the source is 40 Hz

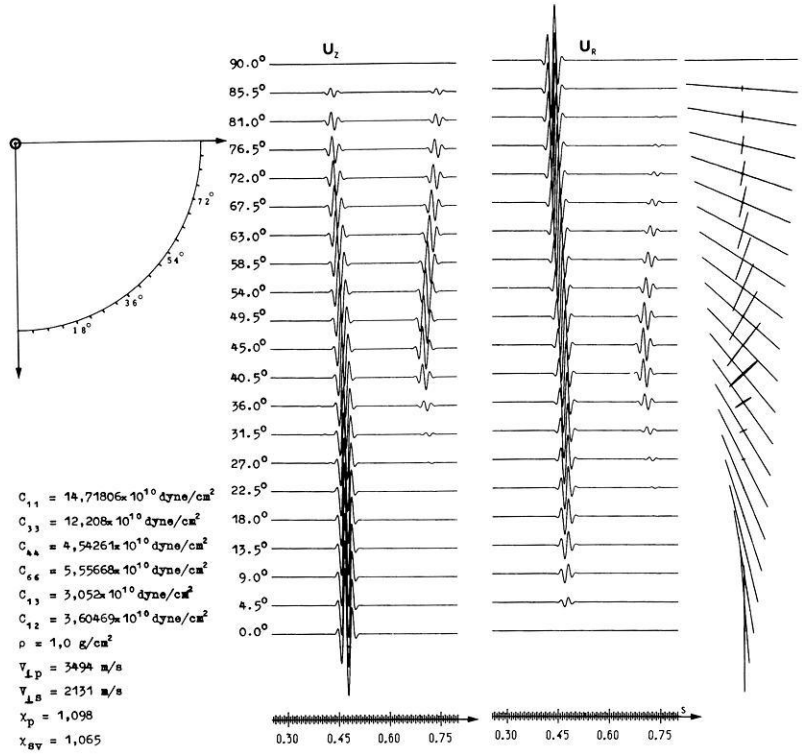

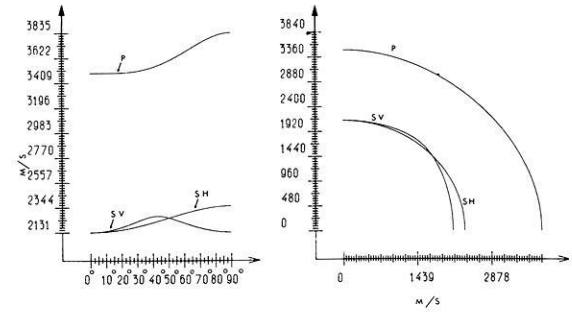

Fig. 2. Theoretical seismograms and parameters of a transversely isotropic model medium. The seismograms are calculated along the radius $R=1.5$ km. The dominant frequency is 40 Hz

One-dimensional problems for fixed values of k_i can be solved simultaneously using multiprocessor computers. Convergence of series (7) and (9) depends on the manner of decreasing the spectrum of the impulse $f(t)$ in the source; for more details see Martynov and Mikhailenko (1984). This approach makes it possible to compute complete theoretical seismograms including nonray waves.

2.1. Examples of calculation of complete theoretical seismograms for transversely isotropic media

Let us discuss some models of anisotropic media, which are common in seismic prospecting. There are three classes of variation in the quasi-longitudinal velocities:

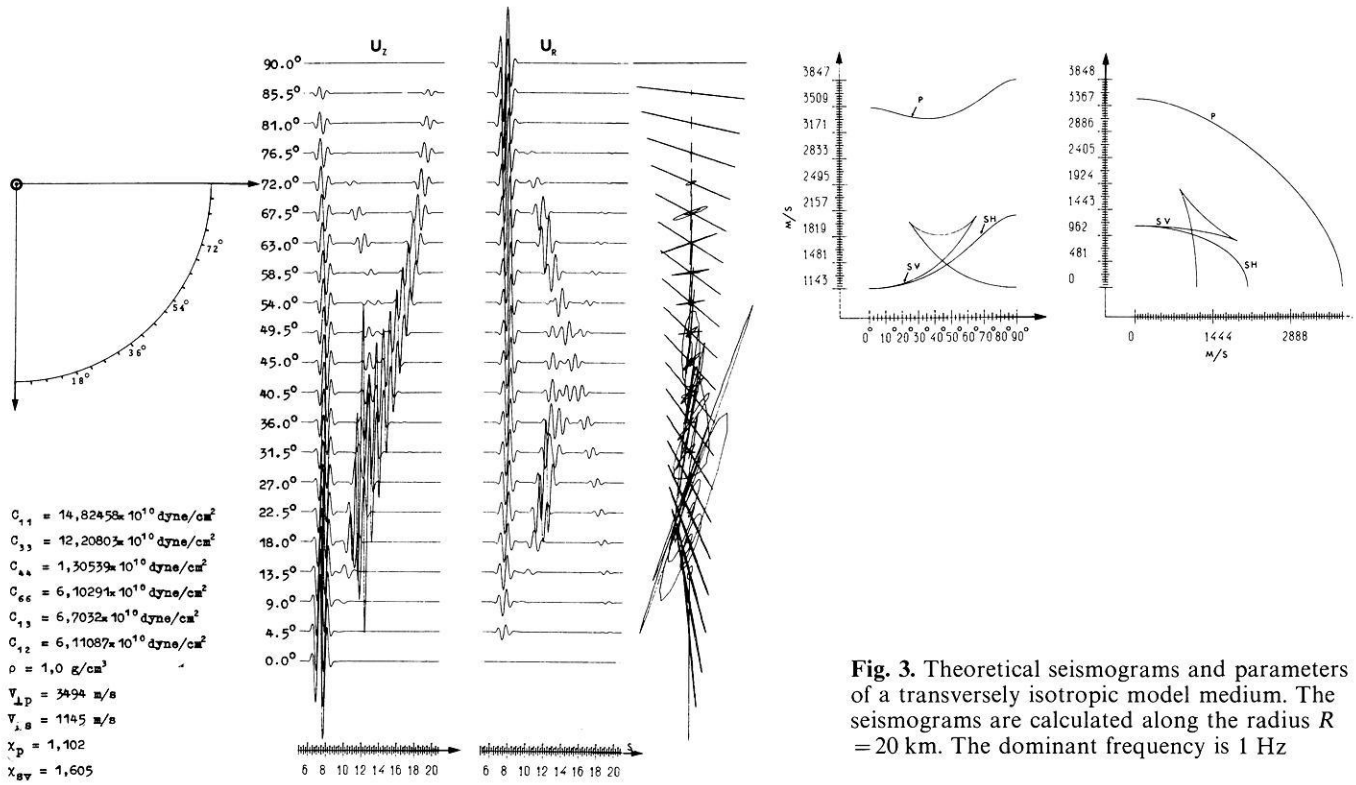

Fig. 3. Theoretical seismograms and parameters of a transversely isotropic model medium. The seismograms are calculated along the radius $R = 20$ km. The dominant frequency is 1 Hz

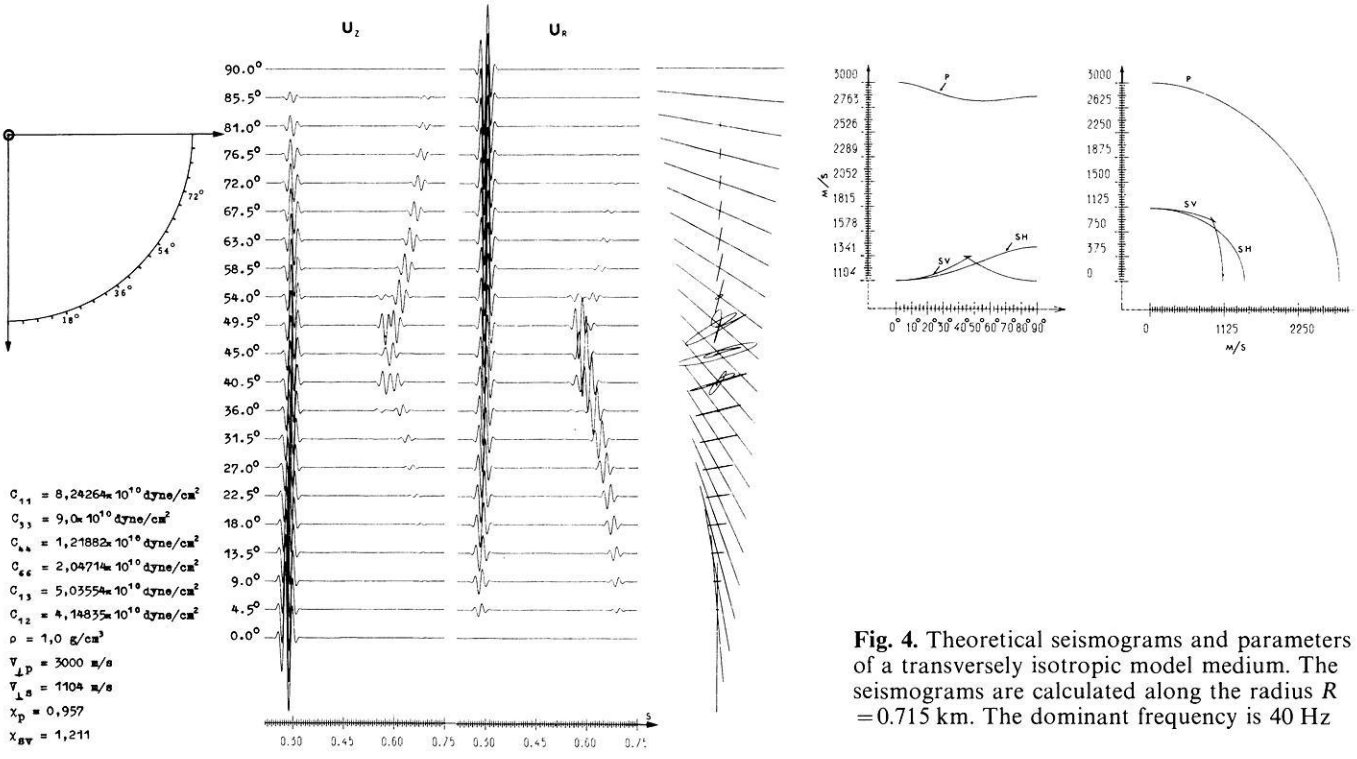

Fig. 4. Theoretical seismograms and parameters of a transversely isotropic model medium. The seismograms are calculated along the radius $R = 0.715$ km. The dominant frequency is 40 Hz

Class I – V_p gradually increases from $V_p(\perp)$ to $V_p(\parallel)$, where $V_p(\perp)$, $V_p(\parallel)$ are velocities in vertical and horizontal directions, respectively.
Class II – V_p has constant value in the range of $\theta = 0°$–$20°$ and then increases to $V_p(\parallel)$.
Class III – V_p decreases and then increases to $V_p(\parallel)$, so an intermediate minimum is observed.

Theoretical seismograms for these models, wave surfaces and polarization diagrams are given in Figs. 1, 2 and 3. The seismograms have been computed along a semicircle with the radius R for an explosive-type source in an anisotropic homogeneous space. The common feature of the figures is that some branches of wave surfaces are not distinctly traced in the theoretical seismograms. Figure 4 illustrates a model of the medium for the case when V_p decreases to $V_p(\parallel)$. Polarization diagrams show elliptic polarization of a quasi-shear wave in the vicinity of the angle of 40°.

The above approach allows us to calculate complete theoretical seismograms for anisotropic media containing a large number of anisotropic inhomogeneous layers. The study of the physics of seismic wave propagation in anisotropic media and comparison to field experiments will allow us to understand in more detail the nature of waves in anisotropic media.

3. Calculation of complete theoretical seismograms for liquid-filled porous media

Let us discuss a model of the porous medium. This physical model became popular for the description of seismic wave propagation in marine sediments and, also, for direct hydrocarbon detection.

In numerical simulation of wave propagation in porous media we take Biot-Frenkel's system of equations in cylindrical coordinates (r, z). For elasticity, this system consists of four equations in partial derivatives.

For the sake of simplicity we will only consider propagation of P waves in the porous medium (a non-dissipative case).

The system of equations is of the form

$$P \cdot \Delta U + Q \cdot \Delta V = \frac{\partial}{\partial t^2}(\rho_{11} U + \rho_{12} V), \tag{16}$$

$$Q \cdot \Delta U + R \cdot \Delta V = \frac{\partial}{\partial t^2}(\rho_{12} U + \rho_{22} V), \tag{17}$$

where U is the displacement in the solid, and V the displacement in the liquid.

Biot's coefficients P, Q, R $(P = \lambda + 2\mu)$ obey the inequality

$$PR - Q^2 > 0.$$

The coefficients $\rho_{11}, \rho_{12}, \rho_{22}$ satisfy the inequalities

$$\rho_{11} > 0, \quad \rho_{22} > 0, \quad \rho_{12} > 0$$

$$\rho_{11}\rho_{22} - \rho_{12}^2 > 0.$$

The point source emitting the P wave is located inside the medium or at the surface $z = 0$. In the latter case, the boundary conditions are of the form

$$\left.\frac{\partial U}{\partial z}\right|_{z=0} = \frac{1}{2\pi}\frac{\delta(r)}{r}\alpha f(t), \tag{18}$$

$$\left.\frac{\partial V}{\partial z}\right|_{z=0} = \frac{1}{2\pi}\frac{\delta(r)}{r}\beta f(t). \tag{19}$$

The problem is solved with zero initial data.

We now turn our attention to the discussion of the third stage of solution, that is selection of the efficient algorithm. To solve problem (16)–(19) we apply the same algorithm which we used in the case of anisotropic media. Let us use the finite Hankel transform along the coordinate r in the form

$$S(z, k_i, t) = \int_0^a U \cdot r J_0(k_i r)\, dr, \tag{20}$$

$$U(z, r, t) = \frac{2}{a^2}\sum_{i=1}^{\infty} S \frac{J_0(k_i r)}{[J_1(k_i a)]^2}, \tag{21}$$

$$F(z, k_i, t) = \int_0^a V \cdot r J_0(k_i r)\, dr, \tag{22}$$

$$V(z, r, t) = \frac{2}{a^2}\sum_{i=1}^{\infty} F \frac{J_0(k_i r)}{[J_1(k_i a)]^2}, \tag{23}$$

where k_i are the roots of the equation $J_0(k_i a) = 0$.

As earlier, we assume at the boundary $r = a$ conditions of the form

$$U|_{r=a} = V|_{r=a} = 0. \tag{24}$$

The new problem of reduced dimensionality is of the form

$$\frac{\partial^2 S}{\partial z^2} - k_i^2 S = \left(\frac{R\rho_{11} - Q\rho_{12}}{PR - Q^2}\right)\frac{\partial^2 S}{\partial t^2} + \left(\frac{R\rho_{12} - Q\rho_{22}}{PR - Q^2}\right)\frac{\partial^2 F}{\partial t^2}, \tag{25}$$

$$\frac{\partial^2 F}{\partial z^2} - k_i^2 F = \left(\frac{P\rho_{12} - Q\rho_{11}}{PR - Q^2}\right)\frac{\partial^2 S}{\partial t^2} + \left(\frac{P\rho_{22} - Q\rho_{12}}{PR - Q^2}\right)\frac{\partial^2 F}{\partial t^2}, \tag{26}$$

$$\left.\frac{\partial S}{\partial z}\right|_{z=0} = (1 - f_0)\frac{f(t)}{2\pi}, \quad \left.\frac{\partial F}{\partial z}\right|_{z=0} = f_0 \frac{f(t)}{2\pi}, \tag{27}$$

$$S|_{t=0} = F|_{t=0} = \left.\frac{\partial S}{\partial t}\right|_{t=0} = \left.\frac{\partial F}{\partial t}\right|_{t=0} = 0. \tag{28}$$

Problem (25)–(28) with fixed values of k_i is solved by the finite difference technique. The scheme used here is explicit with a truncation error of second order with respect to time and space. The displacements U and V are calculated by summing up series (21) and (23).

As an example we took P-wave propagation in a porous medium. At present, this algorithm without essential changes is used for solving Lamb's problem for the vertically inhomogeneous porous medium, with porosity also changing with depth. In this case, the initial problem by means of the finite integral Hankel transformations reduces to a system of four one-dimensional equations with variable coefficients. This system is numerically solved.

3.1. Examples of calculation of theoretical seismograms for a liquid-filled porous medium

Dynamics of seismic-wave propagation in a porous medium has some peculiarities. There are two types of longitudinal waves, the so-called "fast" wave (P_f wave)

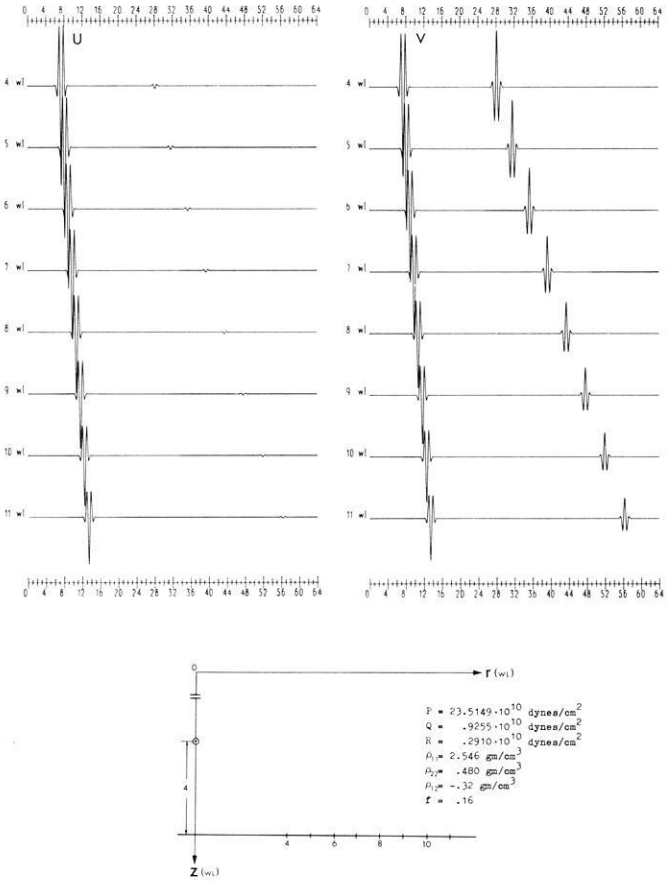

Fig. 5. Theoretical seismograms of P waves in a homogeneous porous medium and parameters of a porous medium. Here U is displacement in the solid, and V is discplacement in the liquid. Receivers are located at a distance of $4\,WL$ below the explosive-type source

and the "slow" wave (P_s wave). The velocity of the slow P_s wave can be greater, equal to or less than that of the shear wave, depending on the relative values of the Biot constants. Examples of calculation of these waves are shown in Fig. 5. The left-hand side of the figure shows the displacement U in the solid; the displacement in the liquid V is shown in the right-hand side. As is seen from the figure, the fast logitudinal wave (P_f wave) is recorded in the first arrivals; in the second arrivals the slow P_s wave is recorded. The longitudinal slow wave is of diffusive nature. As is seen from the figure, the displacement of this wave in the solid and in the liquid are in the opposite phases.

There is a number of physical experiments where the slow longitudinal wave is discovered (see, for example, Coussy and Bourbie, 1984). The question arises: What media can be well described with the help of the Biot-Frenkel theory? This problem requires further investigation both in theory and in practice. In the first place, it is necessary to determine Biot's coefficients for different geological rocks.

4. Calculation of complete theoretical seismograms in non-elastic media

While seismic waves propagate in real media, absorp tion takes place and changes their spectrum and waveform. One should take these features into account when constructing a mathematical model of real media. In this case, the relation between stresses and deformations differs from Hooke's law. We will discuss a class of models describing linear nonelastic media. Here deformation and stress tensors are connected by linear integral differential relations. Such models are suitable for the description of seismic waves far away from the source.

Let us consider Boltzmann's model. The system of elasticity equations in cylindrical coordinates (r, z) is of the form

$$(\Lambda+2M)\left(\frac{\partial^2 U_r}{\partial r^2}+\frac{1}{r}\frac{\partial U_r}{\partial r}-\frac{U_r}{r^2}\right)+\Lambda\frac{\partial^2 U_z}{\partial z\,\partial r}+\frac{\partial}{\partial z}\left[M\left(\frac{\partial U_r}{\partial z}+\frac{\partial U_z}{\partial r}\right)\right]=\rho\frac{\partial^2 U_r}{\partial t^2}-\rho F_r\cdot f(t), \tag{29}$$

$$M\left(\frac{\partial^2 U_r}{\partial z\,\partial r}+\frac{1}{r}\frac{\partial U_r}{\partial z}+\frac{\partial^2 U_z}{\partial z^2}+\frac{1}{r}\frac{\partial U_z}{\partial r}\right)+\frac{\partial}{\partial z}\left[\Lambda\left(\frac{\partial U_r}{\partial r}+\frac{U_r}{r}\right)+(\Lambda+2M)\frac{\partial U_z}{\partial z}\right]=\rho\frac{\partial^2 U_z}{\partial t^2}-\rho F_z f(t), \tag{30}$$

where Λ and M are integral operators of the form

$$\Lambda\cdot x(t)=\lambda\cdot x(t)-\lambda'\int_{-\infty}^{t} g(t-\tau)\,x(\tau)\,d\tau, \tag{31}$$

$$M\cdot y(t)=\mu\cdot y(t)-\mu'\int_{-\infty}^{t} h(t-\tau)\,y(\tau)\,d\tau. \tag{32}$$

Elastic constants λ, μ and nonelastic ones λ', μ' are arbitrary functions of the variable z.

The problem is solved under the following boundary conditions:

$$\tau_{rz}|_{z=0}=M\left(\frac{\partial U_r}{\partial z}+\frac{\partial U_z}{\partial r}\right)\Big|_{z=0}=0, \tag{33}$$

$$\sigma_z|_{z=0}=\Lambda\left(\frac{\partial U_z}{\partial z}+\frac{\partial U_r}{\partial r}+\frac{U_r}{r}\right)+2M\frac{\partial U_z}{\partial z}\Big|_{z=0}=0, \tag{34}$$

with zero initial data

$$U_r=\frac{\partial U_r}{\partial t}=U_z=\frac{\partial U_z}{\partial t}\Big|_{t=0}=0. \tag{35}$$

For an explosive-type source we have

$$F_z=\frac{\delta(r)}{2\pi r}\frac{d}{dz}\delta(z-d), \qquad F_r=\frac{1}{2\pi}\frac{d}{dr}\frac{\delta(r)}{r}\delta(z-d). \tag{36}$$

As earlier, we employ the finite Hankel integral transform:

$$R(z,k_i,t)=\int_0^a r\,U_z(z,r,t)\,J_0(k_i r)\,dr, \tag{37}$$

$$U_z(z,r,t)=\frac{2}{a^2}\sum_{i=1}^{\infty} R(z,k_i,t)\frac{J_0(k_i r)}{[J_0(k_i a)]^2}, \tag{38}$$

$$S(z,k_i,t)=\int_0^a r\,U_r(z,r,t)\,J_1(k_i r)\,dr, \tag{39}$$

$$U_r(z,r,t)=\frac{2}{a^2}\sum_{i=1}^{\infty} S(z,k_i,t)\frac{J_1(k_i r)}{[J_0(k_i a)]^2}. \tag{40}$$

We arrive at the following problem of reduced dimensionality:

$$\rho\frac{\partial^2 S}{\partial t^2}=\frac{\partial}{\partial z}\left(M\frac{\partial S}{\partial z}\right)-k_i^2(\Lambda+2M)S-k_i\frac{\partial}{\partial z}(M\cdot R)$$
$$-k_i\Lambda\frac{\partial R}{\partial z}+\rho f_r\cdot f(t) \tag{41}$$

$$\rho\frac{\partial^2 R}{\partial t^2}=\frac{\partial}{\partial z}\left(\Lambda+2M\frac{\partial R}{\partial z}\right)-k_i^2 M\cdot R+k_i\frac{\partial}{\partial z}(\Lambda\cdot S)$$
$$+k_i M\frac{\partial S}{\partial z}+\rho f_z\cdot f(t), \tag{42}$$

$$M\left(\frac{\partial S}{\partial z}-k_i R\right)\Big|_{z=0}=0, \tag{43}$$

$$(\Lambda+2M)\frac{\partial R}{\partial z}+k_i\Lambda S|_{z=0}=0, \tag{44}$$

$$S=\frac{\partial S}{\partial t}=R=\frac{\partial R}{\partial t}\Big|_{t=0}=0, \tag{45}$$

where k_i are the roots of Bessel's equation $J_1(k_i a)=0$.

Applying transformations of the form (37)–(40) brings about new boundary conditions of the form

$$U_r|_{r=a}=\frac{\partial U_z}{\partial r}\Big|_{r=a}=0. \tag{46}$$

We will consider the problem up to the time $t=T$, where T is the minimal time of longitudinal wave propagation to the reflecting surface at $r=a$.

Let us apply a finite integral transform with respect to the variable t in the one-dimensional problem obtained. The possibility to apply these transforms for the problem under consideration has been studied in Fatianov and Mikhailenko (1979), Fatianov (1980). Let us apply the finite Fourier transform

$$x(k_i,n,z)=\int_0^{2T} S(z,k_i,t)\,e^{-i\lambda_n t}\,dt, \tag{47}$$

$$y(k_i,n,z)=\int_0^{2T} R(z,k_i,t)\,e^{-i\lambda_n t}\,dt, \tag{48}$$

$$S(z,k_i,t)=\frac{1}{T}\left[\frac{a}{2}+\sum_{n=1}^{\infty} a\cdot\cos\lambda_n t+b\sin\lambda_n t\right], \tag{49}$$

$$R(z,k_i,t)=\frac{1}{T}\left[\frac{c}{2}+\sum_{n=1}^{\infty} c\cdot\cos\lambda_n t+d\sin\lambda_n t\right], \tag{50}$$

$$\lambda_n=\frac{n\pi}{T},$$

$$a(k_i,n,z)=\mathrm{Re}\,x(k_i,n,z),\qquad c(k_i,n,z)=\mathrm{Re}\,y(k_i,n,z),$$
$$b(k_i,n,z)=-\mathrm{Im}\,x(k_i,n,z),\qquad d(k_i,n,z)=-\mathrm{Im}\,y(k_i,n,z).$$

to Eqs. (41) and (42). As a result we obtain a system of ordinary differential equations

$$\frac{d}{dz}\left[c_1\frac{dx}{dz}-k_i c_1 y\right]-k_i^2(c_2+2c_1)x-k_i c_2\frac{dy}{dz}$$
$$+\rho\lambda_n^2 x+\rho f_r\cdot p=0, \tag{51}$$

$$\frac{d}{dz}\left[(c_2+2c_1)\frac{dy}{dz}+k_i c_2 x\right]-k_i^2 c_1 y+k_i c_1\frac{dx}{dz}$$
$$+\rho\lambda_n^2 y+\rho\cdot f_z\cdot p=0 \tag{52}$$

with boundary conditions

$$k_i c_2 x+(c_2+2c_1)\frac{dy}{dz}\Big|_{z=0}=0,\qquad c_1\left(\frac{dx}{dz}-k_i y\right)\Big|_{z=0}=0 \tag{53}$$

$$x|_{z=b}=0,\qquad y|_{z=b}=0. \tag{54}$$

Here

$$c_1=\mu-\mu'\beta_n,\qquad c_2=\lambda-\lambda'\cdot\alpha_n,$$

$$p=\int_0^{2T} f(t)\,e^{-i\lambda_n t}\,dt,\qquad \alpha_n=\int_0^{2T} g(\tau)\,e^{-i\lambda_n\tau}\,d\tau,$$

$$\beta_n=\int_0^{2T} h(\tau)\,e^{-i\lambda_n\tau}\,d\tau.$$

In Eqs. (51) and (52) we assume that the conditions

$$\frac{\partial S}{\partial t}+i\lambda_n S|_{t=2T}\approx 0,\qquad \frac{\partial R}{\partial t}+i\lambda_n R|_{t=2T}\approx 0 \tag{55}$$

are approximately met. It can be shown that these conditions are fulfilled with high accuracy if the duration (l) of an impulse in the source is much less than the value $2T$ ($l\ll 2T$).

Problem (51)–(54) is solved numerically for different sets of k_i and n. After that we obtain the displacement components by summing up series (49), (50) and (38), (40). Problem (51) can be accurately solved for layered homogeneous media (see Fatianov and Mikhailenko, 1984).

4.1. Examples of calculation of complete theoretical seismograms for Boltzmann's media

Attenuation of seismic waves has become an important parameter in seismic exploration in recent years. Experimental studies of attenuation properties of real media show the linearity with the frequency of the damping factor α over a wide frequency range. This fact was taken into consideration in numerical simulation of seismic waves in nonelastic inhomogeneous media.

Note that in seismic exploration one uses the damping factor α and the logarithmic decrement Δ. In our equations, properties of the medium are determined by nonelastic coefficients λ', μ' and kernels $g(\xi)$, $h(\xi)$. There are particular formulas which relate the nonelastic coefficients λ', μ' to the damping factor α or logarithmic decrement Δ.

The form of the functions $g(\xi)$ and $h(\xi)$ can be arbitrarily selected. For example, if

$$h(\xi)=g(\xi)=\begin{cases}e^{-\lambda\xi}, & \xi>0,\\ 0\end{cases}$$

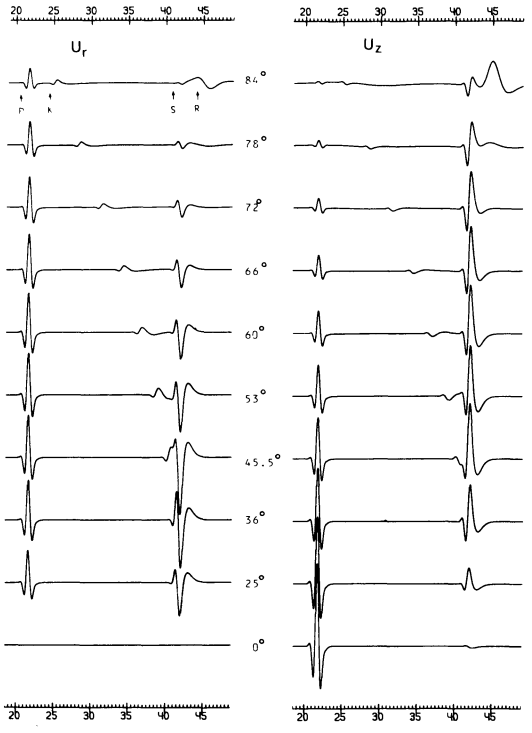

Fig. 6. Theoretical seismograms of the horizontal and vertical components of displacement for homogeous Maxwell's model. Attenuation decrements of P and S waves are equal. $\Delta_P=\Delta_S=0.1$, $V_S/V_P=0.5$. The seismograms are calculated along the radius $R=20\,WL$, where WL is the dominant P wavelength. Here: P - longitudinal wave, S - shear wave, R - Rayleigh wave, K - head wave

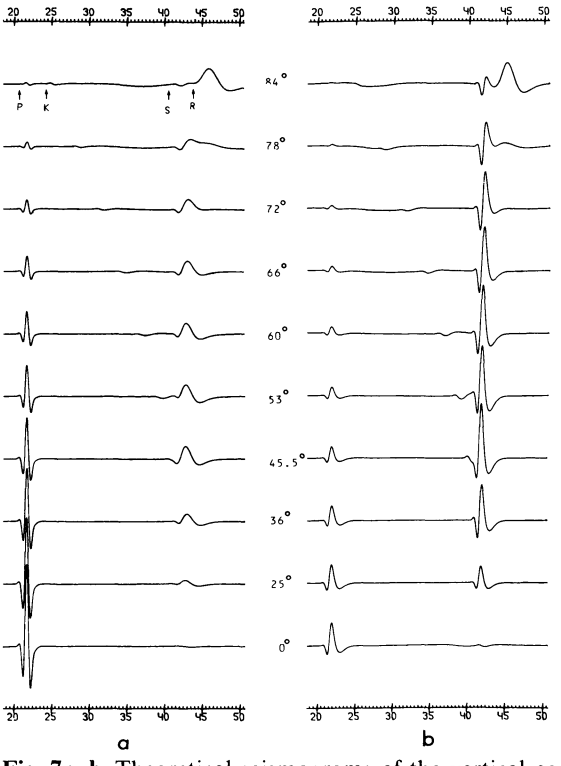

Fig. 7a, b. Theoretical seismograms of the vertical component of displacement for homogeneous Maxwell's model in case of: **(a)** $\Delta_P/\Delta_S=0.5$, $\Delta_P=0.1$; **(b)** $\Delta_P/\Delta_S=2$, $\Delta_S=0.1$. The seismograms are calculated along the radius $R=20\,WL$

we have the Maxwell medium. If the functions $g(\xi)$ and $h(\xi)$ are connected by the relation

$$3\cdot\lambda' g+2\mu'\cdot h=0$$

and

$$h(\xi)=\begin{cases}e^{-\gamma\xi}, & \xi>0,\\ 0\end{cases}$$

we arrive at Deriagin's model (Deriagin, 1931). Thus, by varying the form of the function $g(\xi)$ and $h(\xi)$ we will obtain different models of media.

We now consider the Maxwell model. Let the source be a vertical force acting at the free surface of the homogeneous half-space. Figure 6 shows theoretical seismograms of the vertical and horizontal displacement components calculated at a radius $R=20\,WL$, where WL is the dominant wavelength P. The decrements of attenuation of P and S waves are $\Delta_s=\Delta_p=0.1$, $v_s/v_p=0.5$.

As compared to the elastic medium, the wave picture essentially changes. The variations of wave amplitudes with the angle, correspond on the whole to the elastic medium case but the waveforms undergo considerable changes.

The waveform of the P wave becomes similar to the integral of the P wave waveform in the elastic medium. The S wave spectrum is shifted towards low frequencies as compared to P waves.

Experimental data show evidence of the wide range of variation of the ratio v_p/v_s. Its value can be equal to 1, or can be more or less than 1. Figure 7 represents theoretical seismograms of the vertical displacement components for the following two cases:

(a) $\Delta_p/\Delta_s=0.5$ $\quad\Delta_p=0.1$
(b) $\Delta_p/\Delta_s=2$ $\quad\Delta_s=0.1$

As is seen from the figure, with the relation Δ_p/Δ_s changing, redistribution of energy between P and S waves takes place.

Figure 8a and b shows theoretical seismograms in the presence of a thin layer inside the half-space. The thickness of the layer is $h=0.4\,WL$. The source of explosive type is located at a distance of $d=0.2\,WL$ from the free surface. The parameters of the medium are $v_{s_1}/v_{p_1}=0.5$, $v_{p_2}=2v_{p_1}$, $v_{s_2}/v_{p_2}=0.5$. Figure 8a represents the theoretical seismograms for the elastic medium and Fig. 8b shows the theoretical seismograms for a Maxwell medium in the layer and the half-space. Here

$$\Delta_{s_1}=\Delta_{p_1}=0.4,\quad v_{s_2}/v_{p_2}=0.5,\quad \Delta_{p_2}=0.01.$$

Figure 8a and b represents synthetic seismograms of the vertical component for different epicentral distances. The seismograms have been calculated at the free surface. The wave picture is of complicated character due to interference in the layer. As we can judge

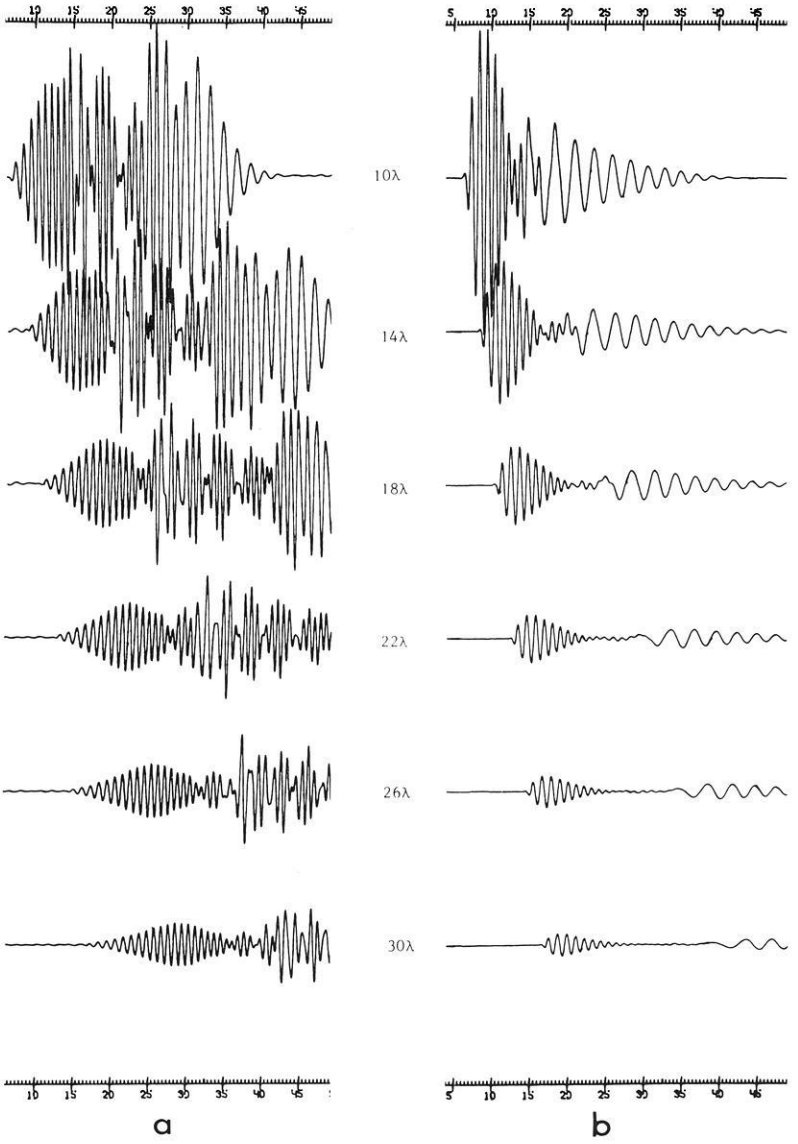

Fig. 8a, b. Theoretical seismograms of the vertical component for a model of a thin high-velocity layer in a half-space. The layer thickness is $h=0.4\ WL$. An explosive-type source is located in the middle of the layer. Parameters of the medium $V_{P_2}=2V_{P_1}$, $V_{S_1}/V_{P_1}=0.5$, $V_{S_2}/V_{P_2}=0.5$. The following cases are shown: **(a)** elastic medium; **(b)** Maxwell's medium with parameters $\Delta_{S_1}=\Delta_{P_1}=0.4$, $\Delta_{P_2}=\Delta_{S_2}=0.5$, $\Delta_{P_2}=0.01$. The ratio of scales of theoretical seismograms for **(a)** and **(b)** is 1:8

from the figures, attenuation changes essentially the wave picture.

5. Calculation of complete theoretical seismograms for complex subsurface geometries

We have considered three-dimensional axisymmetrical problems for one-dimensional models of media. However, one-dimensional models are not sufficient for the description of real media. In numerical modelling it is necessary to take the 2-D and 3-D models of media into consideration, but this problem is far from being simple. The basic problem here is to construct efficient algorithms for calculation of complete theoretical seismograms for 2-D and 3-D models of media.

Here we will generalize the above-mentioned algorithms developed for one-dimensional models for two-dimensional models with arbitrary dependence of elastic parameters on two spatial coordinates. Two variations of this algorithm were suggested some years ago (Mikhailenko, 1978, 1979), and were developed in a series of papers in the USSR (see, for example, Mikhailenko and Korneev, 1983). The review of some of the results obtained has been published in English (Mikhailenko, 1984; Mikhailenko and Korneev, 1984).

We will start in the following with the equation of motion for horizontally polarized shear (*SH*) waves in Cartesian coordinates x and z. Here the elastic parameters are arbitrary functions of two spatial coordinates. A line source is located inside the half-space. Further, we will discuss the plane problem of *P-SV*-wave propagation in a two-dimensional inhomogeneous half-space (Lamb's problem).

In realistic field experiments point sources which generate spherical waves are used. Thus, amplitudes of reflected and diffracted waves are not only affected by reflection coefficients, but also by spherical divergence. Therefore, we will also consider *P*- and *SV*-wave propagation in a three-dimensional half-space, when the elastic parameters are arbitrary functions of two spatial coordinates.

Finally, we will illustrate these cases by examples of calculation of complete theoretical seismograms for *SH*

waves and *P-SV* waves for complex subsurface geometries.

5.1. *SH-wave propagation in complex subsurface geometries*

Let us consider an elastic half-space in a Cartesian coordinate system, where the *SH*-wave velocity $v_s(x,z)$ is an arbitrary function of two coordinates. For the sake of simplicity, the density ρ of the medium is taken constant. In such a medium *SH*-wave propagation from a line source, located at $x=x_0$, $z=z_0$ is given by the equation

$$\frac{\partial}{\partial x}\left(v_s^2\frac{\partial U}{\partial x}\right)+\frac{\partial}{\partial z}\left(v_s^2\frac{\partial U}{\partial z}\right)=\frac{\partial^2 U}{\partial t^2} +F_1(x-x_0)F_2(z-z_0)f(t) \tag{56}$$

with the boundary condition

$$\left.\frac{\partial U}{\partial z}\right|_{z=0}=0 \tag{57}$$

and the initial values

$$U|_{t=0}=\left.\frac{\partial U}{\partial t}\right|_{t=0}=0. \tag{58}$$

Here the function $f(t)$ represents the time variation of the source. For a finite source, the functions $F_1(x-x_0)$, $F_2(z-z_0)$ are in the form of the Gauss function

$$F_1(x-x_0)=\sqrt{\frac{n_0}{\pi}}e^{-n_0(x-x_0)^2},$$

$$F_2(z-z_0)=\sqrt{\frac{m_0}{\pi}}e^{-m_0(z-z_0)^2}. \tag{59}$$

For $n_0, m_0\to\infty$ the functions F_1 and F_2 tend toward deltafunctions.

Problem (56)–(59) will now be solved with two versions of the algorithm.

First version of the algorithm. This version is based on a combination of finite integral Fourier transforms with respect to one of the spatial coordinates (e.g., the coordinate corresponding to the epicentral distance) and the finite difference method. In this case the problem reduces to solving a system of equations with partial derivatives with respect to one spatial coordinate (say, the vertical one) with coefficients which are finite Fourier integrals of the elastic parameters varying along the epicentral coordinate. This approach is an extension of the standard techniques of separation of variables to the solution of problems of complex subsurface geometries. For the application of the finite integral Fourier transform we introduce the boundary conditions for $x=0$ and $x=b$,

$$\left.\frac{\partial U}{\partial x}\right|_{x=0}=\left.\frac{\partial U}{\partial x}\right|_{x=b}=0. \tag{60}$$

We select a sufficiently large distance b and consider the wave field up to the time $t=T$, where T is the minimal time of propagation of the wavefront to the reflecting surface.

Now, we apply the finite integral Fourier transform along the coordinate x from 0 to b:

$$R(z,n,t)=\int_0^b U(z,x,t)\cos\frac{n\pi x}{b}dx, \tag{61}$$

$$U(z,x,t)=\frac{1}{b}R(z,0,t)+\frac{2}{b}\sum_{n=1}^{\infty}R(z,n,t)\cos\frac{n\pi x}{b}. \tag{62}$$

We then multiply both parts of Eq. (56) by $\cos\frac{n\pi x}{b}$ and integrate from 0 to b. If we integrate by parts the first term of Eq. (56), we arrive at an equation of the form

$$\frac{\partial^2 R}{\partial t^2}=\frac{n\pi}{b}\int_0^b v_s^2\frac{\partial U}{\partial x}\sin\frac{n\pi x}{b}dx+\int_0^b\frac{\partial}{\partial z}\left(v_s^2\frac{\partial U}{\partial z}\right)\cos\frac{n\pi x}{b}dx -F_2(z-z_0)e^{-\frac{n^2\pi^2}{4b^2n_0}}\cos\frac{n\pi x_0}{b}f(t). \tag{63}$$

Integrating the same term once more, we obtain

$$\frac{\partial^2 R}{\partial t^2}=-\left(\frac{n\pi}{b}\right)^2\int_0^b v_s^2 U\cos\frac{n\pi x}{b}dx -\frac{n\pi}{b}\int_0^b \dot{v}_s^2 U\sin\frac{n\pi x}{b}dx +\int_0^b\frac{\partial}{\partial z}\left(v_s^2\frac{\partial U}{\partial z}\right)\cos\frac{n\pi x}{b}dx -F_2(z-z_0)e^{-\frac{n^2\pi^2}{4b^2n_0}}\cos\frac{n\pi x_0}{b}f(t). \tag{64}$$

Here $\dot{v}_s^2$ is the derivative of the squared velocity with respect to x.

There is no separation of variables in Eqs. (63) and (64) since velocity $v_s(x,z)$ is an arbitrary function of two spatial coordinates. Note, that Eq. (63) contains the first derivative of displacement with respect to x under the integral sign, and Eq. (64) the displacement itself.

In recent years several different problems in mathematical physics and seismology have been solved using an orthogonal set of trigonometric functions instead of a finite-difference expression to approximate a spatial derivative (see, for example, Kreiss and Oliger, 1972; Gazdag, 1973, 1981). This approach allows for a highly precise calculation of spatial derivatives, but requires substantially more CPU time per degree of freedom. This difficulty is reduced with the use of the fast Fourier transform (FFT) and array processors, which are ideal for the task of calculating spatial derivatives.

Approximating the spatial derivative $\frac{\partial U}{\partial x}$ in Eq. (63) by the Fourier series (62), we obtain the following system of equations:

$$\frac{\partial^2 R(z,m,t)}{\partial t^2}=-\frac{n\pi^2}{b^2}\sum_{m=0}^{\infty}R(z,m,t)\,m \cdot\frac{2}{b}\int_0^b v_s^2(x,z)\sin\frac{m\pi x}{b}\sin\frac{n\pi x}{b}dx +\sum_{m=0}^{\infty}\frac{2}{b}\int_0^b\frac{\partial}{\partial z}\left[v_s^2(x,z)\frac{\partial R(z,m,t)}{\partial z}\right] \cdot\cos\frac{m\pi x}{b}\cos\frac{n\pi x}{b}dx -F_2(z-z_0)e^{-\frac{n^2\pi^2}{4b^2n_0}}\cos\frac{n\pi x_0}{b}f(t). \tag{65}$$

Equation (64) does not contain the spatial derivative of the displacement $U(z,x,t)$ with respect to x. In this case we approximate the function itself by series (62) and obtain another system of equations:

$$\frac{\partial^2 R(z,n,t)}{\partial t^2} = -\left(\frac{n\pi}{b}\right)^2 \sum_{m=0}^{\infty} R(z,m,t) \cdot \frac{2}{b}\int_0^b v_s^2(x,z)\cos\frac{m\pi x}{b}\cos\frac{n\pi x}{b}\,dx - \left(\frac{n\pi}{b}\right)\sum_{m=0}^{\infty} R(z,m,t)\,\frac{2}{b}\int_0^b v_s^2(x,z)\cos\frac{m\pi x}{b}\sin\frac{n\pi x}{b}\,dx + \sum_{m=0}^{\infty}\frac{2}{b}\int_0^b \frac{\partial}{\partial z}\left[v_s^2(x,z)\frac{\partial R(z,m,t)}{\partial z}\right]\cdot\cos\frac{m\pi x}{b}\cos\frac{n\pi x}{b}\,dx - F_2(z-z_0)\,e^{-\frac{n^2\pi^2}{4b^2 n_0}}\cos\frac{n\pi x_0}{b} f(t). \tag{66}$$

It is not quite clear right now which one of these two systems is preferable. At first sight system (65) seems more convenient for numerical implementation, although convergence of system (66) is better since the term m is absent under the summation sign.

Below we will deal with system (65). This system is solved with the boundary conditions

$$\left.\frac{\partial R(z,n,t)}{\partial z}\right|_{z=0} = \left.\frac{\partial R(z,n,t)}{\partial z}\right|_{z=a} = 0 \tag{67}$$

with zero initial data

$$R(z,n,t)|_{t=0} = \left.\frac{\partial R(z,n,t)}{\partial t}\right|_{t=0} = 0. \tag{68}$$

Problem (65), 67), (68) is solved with the help of finite-difference techniques. The scheme used here is explicit, with a truncation error of the second order with respect to time and space. System (65) in a finite difference form can be written as

$$\frac{1}{\Delta t^2}[R_k^{p+1}(n) - 2R_k^p(n) + R_k^{p-1}(n)] = -\frac{n\pi^2}{b^2}\sum_{m=0}^{\infty} m\cdot R_k^p(m)\cdot D_k(m,n) + \sum_{m=0}^{\infty}\frac{1}{2\Delta z^2}\{[R_{k+1}^p(m) - R_k^p(m)]\,c_{k+1}(m,n) + [R_{k+1}^p(m) - 2R_k^p(m) + R_{k-1}^p(m)]\,c_k(m,n) + [R_k^p(m) - R_{k-1}^p(m)]\,c_{k-1}(m,n)\} - F_{2k}\,e^{-\frac{n^2\pi^2}{4b^2 n_0}}\cos\frac{n\pi x_0}{b} f^p, \tag{69}$$

where $z = k\cdot\Delta z$, $t = p\cdot\Delta t$,

$$D_k(m,n) = \frac{1}{b}\int_0^b v_{s_k}^2(x)\cos\frac{(n-m)\pi x}{b}\,dx - \frac{1}{b}\int_0^b v_{s_k}^2(x)\cos\frac{(n+m)\pi x}{b}\,dx = h_k(n-m) - h_k(n+m), \tag{70}$$

$$c_k(m,n) = h_k(n-m) + h_k(n+m). \tag{71}$$

The infinite system (69) is replaced by a finite system and is solved numerically. The boundary conditions (67) are approximated in a familiar way. For the nodes k of the difference scheme ($z_k = k\cdot\Delta z$), where the velocity v_{s_k} is constant along the lines parallel to the $0x$ axis from 0 to b, system (69) generates into one equation with the parameter n:

$$\frac{1}{\Delta t^2}[R_k^{p+1} - 2R_k^p + R_k^{p-1}] = -\frac{n^2\pi^2}{b^2} v_{s_k}^2 R_k^p + \frac{1}{\Delta z^2}[(R_{k+1}^p - R_k^p)\,v_{s_{k+1}}^2 + (R_{k+1}^p - 2R_k^p + R_{k-1}^p)\,v_{s_k}^2 - (R_k^p - R_{k-1}^p)\,v_{s_{k-1}}^2] - F_{2k}\,e^{-\frac{n^2\pi^2}{4b^2 n_0}}\cos\frac{n\pi x_0}{b} f^p. \tag{72}$$

Note that the velocity v_{s_k} varies from point to point along the coordinate z. Here we have a classical separation of variables in combination with the finite difference approach. This algorithm was suggested and developed by Mikhailenko (1973) and Alekseev and Mikhailenko (1976, 1978, 1980). When the velocity is a function of two coordinates, it is necessary to solve system (69). The coefficients of this system

$$h_k(s) = \frac{1}{b}\int_0^b v_{sk}^2(x)\cos\frac{s\pi x}{b}\,dx, \tag{73}$$

$s = n \pm m$

are analytically calculated. The function $v_s(x)$ which varies arbitrarily from 0 to b is approximated at each of the points on nonuniform intervals by the linear function $v_{s_l} = v_{0_l}(1+\beta_l x)$. Here v_{0_l} is the initial velocity of each interval l, and β is the coefficient of velocity variation, i.e., the velocity gradient.

The complexity of subsurface geometries in the direction of the coordinate x does not cause additional computational difficulties in solving system (69), as long as the interval of integration between 0 and b in (73) is partitioned into a sufficiently large number of segments in which the function $v_s^2(x)$ is well approximated by the linear function defined earlier.

It should be noted that the dimension of the finite system (69) is slightly dependent on the partitioning of the interval 0 to b. The number of terms that are needed to properly approximate the infinite sum in system (69) is dependent on the Fourier spectrum width of the signal $f(t)$. The additional convergence of the series (62) and hence the number of terms which must be used in the series is dependent on the smoothness of the velocity used in integral (73). Therefore, one may use splines of different orders for smoothing the function $h(s)$ (Mikhailenko and Korneev, 1984).

This paper also shows that if the velocity $v_s^2(x,z)$ is of the form (Fig. 9)

$$v_s^2(x,z) = v_0(z) \pm \frac{\Delta v(z)}{2}\left(1 - \cos\frac{l\pi x}{b}\right), \tag{74}$$

the original system (63) degenerates into a differential equation with a shift parameter. Here l is some fixed arbitrary integer.

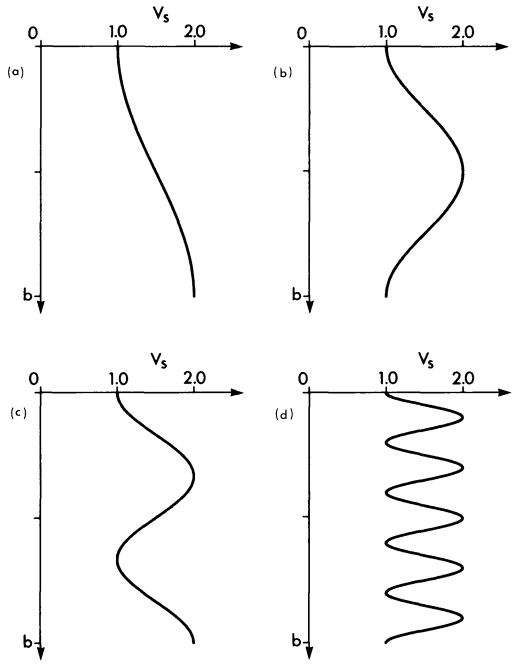

Fig. 9. Variation of the velocity $v_s(x,z)$ given by the formula $v_s^2(x,z)=A(z)+B(z)\cos\frac{l\pi x}{b}$. The values of $A(z)$ and $B(z)$ are constant and the figure shows the dependence of the velocity on x: (a) $l=1$, (b) $l=2$, (c) $l=3$ and (d) $l=10$

In the numerical solution of system (69) with an explicit finite difference scheme most of the computing time is required for the computation of the convolution-type sums

$$\sum_{m=0}^{M} R_k^p(m)\,[h_k(n-m)\pm h_k(n+m)]. \tag{75}$$

These sums may be evaluated using the fast Fourier transform (FFT) or some other particular techniques. It is highly desirable to use an array processor which allows one to substantially decrease the main-frame time requirements for computing synthetic seismograms for complex subsurface geometries. It should be noted that for convolution sums (75) at present more efficient algorithms have been developed as compared to those based on the use of FFT (Nussbaumer, 1981).

Second version of the algorithm. The second version of the algorithm is based on utilization of finite integral Fourier transforms with respect to two spatial coordinates. Let us apply the finite integral cosine transform along the coordinate z from 0 to a

$$W(i,n,t)=\int_0^a R(z,n,t)\cos\frac{i\pi z}{a}\,dz, \tag{76}$$

$$R(z,n,t)=\frac{1}{a}W(0,n,t)+\frac{2}{a}\sum_{i=1}^{\infty} W(i,n,t)\cos\frac{i\pi z}{a} \tag{77}$$

to the system of partial differential equations. We multiply (65) by $\cos\frac{i\pi z}{a}$ and integrate by parts from 0 to a. Performing manipulations similar to those mentioned above and making use of condition (67) we obtain

$$\begin{aligned}\frac{d^2W(i,n,t)}{dt^2}=&-\frac{n\pi}{b}\sum_{m=0}^{\infty}\sum_{j=0}^{\infty}\delta_{mj}\frac{m\pi}{b}W(j,m,t)\cdot D_1(n,m,i,j)\\&-\frac{i\pi}{a}\sum_{m=0}^{\infty}\sum_{j=0}^{\infty}\delta_{mj}\frac{j\pi}{a}W(j,m,t)\,D_2(n,m,i,j)\\&-e^{-\frac{n^2\pi^2}{4b^2n_0}}e^{-\frac{i^2\pi^2}{4a^2i_0}}\cos\frac{n\pi x_0}{b}\cos\frac{i\pi z_0}{a},\end{aligned} \tag{78}$$

where

$$\delta_{mj}=\begin{cases}1 & \text{if } m\neq 0\ j\neq 0\\ \frac{1}{2} & \text{if } m=0\ j\neq 0 \quad\text{or}\quad m\neq 0\ j=0\\ \frac{1}{4} & \text{if } m=j=0\end{cases}$$

$$\begin{aligned}D_1(n,m,i,j)=&\tfrac{1}{4}[h(n-m,i-j)+h(n-m,i+j)\\&-h(n+m,i-j)-h(n+m,i+j),\\D_2(n,m,i,j)=&\tfrac{1}{4}[h(n-m,i-j)-h(n-m,i+j)\\&+h(n+m,i-j)-h(n+m,i+j)],\end{aligned} \tag{79}$$

$$h(r,s)=\frac{4}{ab}\int_0^a\int_0^b v_s^2(x,z)\cos\frac{r\pi z}{a}\cos\frac{s\pi x}{b}\,dx\,dz.$$

System (78) is solved with zero initial values

$$W(i,n,t)|_{t=0}=\left.\frac{dW(i,n,t)}{dt}\right|_{t=0}=0. \tag{80}$$

The infinite system (78) is approximated by a finite system and is solved numerically by means of an explicit difference scheme:

$$\begin{aligned}&\frac{1}{\Delta t^2}[W^{p+1}(i,n)-2W^p(i,n)+W^{p-1}(i,n)]\\&=-\frac{n\pi}{b}\sum_{m=0}^{M-1}\sum_{j=0}^{J-1}\delta_{mj}\frac{m\pi}{b}W^p(j,m)\,D_1(n,m,i,j)\\&\quad-\frac{i\pi}{a}\sum_{m=0}^{M-1}\sum_{j=0}^{J-1}\delta_{mj}\frac{j\pi}{a}W^p(j,m)\,D_2(n,m,i,j)\\&\quad-e^{-\frac{n^2\pi^2}{4b^2n_0}}\cos\frac{n\pi x_0}{b}e^{-\frac{i^2\pi^2}{4a^2i_0}}\cos\frac{i\pi z_0}{a}f(t).\end{aligned} \tag{81}$$

The displacement $U(z,x,t)$ is determined by summing up the series (77) and (62). For the calculation of integral (79) the integration domain from 0 to b and 0 to a is partitioned into nonuniform segments. In each of these segments the velocity is approximated by the bilinear function

$$v_{s_{kl}}=a_{kl}+b_{kl}x+c_{kl}z+d_{kl}xz.$$

The coefficients a_{kl}, b_{kl}, c_{kl} and d_{kl} are determined from the velocity values in the nodes of the rectangle. In this way the value of integral (79) in each segment is easily calculated analytically. If we sum up the values of the integrals for all segments we will obtain the coefficients $h(r,s)$. Due to the fact that the function $v(x,z)$ is continuous at all the boundaries of the segment, the coefficient decreases as $1/(r\pm s)^2$. A discontinuity in the velocity function is well approximated by a gradient layer whose width is much less than the wavelength. The number of segments used for the calculation of the coefficients $h(r,s)$ depends on the complexity of subsurface geometries. Here, the coefficients $h(r,s)$ are calculated with a special subroutine.

In numerical solutions of system (81) double sums of the convolution type

$$\sum_{m=0}^{M-1}\sum_{j=0}^{J-1}\tilde{W}^p(j,m)\cdot h(n\pm m, i\pm j) \tag{82}$$

are calculated with the fast Fourier transform. We may also use some other algorithms (Nussbaumer, 1981).

The use of an array processor considerably reduces the computer time for synthetic seismograms of complex subsurface geometries. The convergence of the double sums of type (82) increases, if one uses splines for approximating the velocity $v_s^2(x,z)$ in calculation of the coefficients $h(r,s)$.

Note that one can avoid the calculation of integral (79) in calculations of the double sums (82) if the velocity $v_s(x,z)$ is assumed to be a sufficiently smooth function of two coordinates. In the case where the velocity $v_s(x,z)$ is given at the nodes of a uniform grid, the number of nodes along the coordinates x and z must coincide with the number of terms to be summed up in (82). For more details see Mikhailenko and Korneev (1984).

The second version of the algorithm described here can be related to the so-called spectral methods. In a recent paper by Kosloff and Baysal (1982) a pseudospectral so-called collocation method was suggested for the calculation of synthetic seismograms. The pseudospectral method is an approximation which uses interpolating functions to evaluate derivatives represented on a grid in physical space. It is called a pseudospectral method because the interpolating functions used are the same as in the spectral method. In the pseudospectral method, all operations except differentiation are carried out in the physical space defined by a grid.

In contrast to the familiar spectral method we gain some advantage in computation time since spectral multiplication is not necessary. The price that is paid for this advantage is that the calculations are aliased. The effect of aliasing may not be important but we must keep in mind that aliasing has implications for the stability of a calculation for long intervals of time (Merilees and Orszag, 1979). Also, the effect of aliasing may be important if the abruptly changing velocity is present in our model.

When we use the pseudospectral method, the elastic parameters are defined at the points of a uniform grid. The FFT dimension in this case is determined by the number of grid points. To approximate a medium with complex subsurface geometries or a medium containing thin layers it is necessary to use a large number of grid points which leads to an essential increase in computation time.

Note that in contrast to the pseudospectral method we do not calculate second spatial derivatives but approximate by the Fourier series either the first spatial derivative or the function itself. This brings about the better convergence of the algorithm.

The second version is suitable for use in calculating synthetic seismograms for very complex subsurface geometries including inhomogeneities which are much smaller than the predominant wavelengths. This approach requires much less capacity of computer main memory than the finite difference method. Although this approach requires more computer time, the use of the FFT makes it possible to overcome this difficulty. The weak point in this approach is the fact that it is difficult to satisfy the boundary conditions at the free surface.

This drawback is absent in the first approach, which for instance is applicable to the calculation of Rayleigh waves in arbitrary two-dimensional inhomogeneous media. This version is most effective for thin-layer models involving heterogeneities whose amplitude along one coordinate (say, the vertical one) is less than along the other. These are models of typical petroleum traps (anticlines, reefs, thrust faults, etc.) whose size in the vertical direction is not greater than 8–10 wavelengths. This approach, as we will discuss later, is used for complex subsurface geometries in a cylindrical coordinate system.

Now we will discuss the implementation of the first approach for the calculation of theoretical seismograms of *P-SV* waves for complex subsurface geometries.

5.2. P- and SV-wave propagation in complex subsurface geometries (Lamb's problem)

Consider Lamb's problem for the elastic inhomogeneous half-space $z\geqq 0$, where the parameters of the medium are arbitrary functions of two spatial variables x and z. For the sake of simplicity we consider the density ρ to be constant. At the boundary $z=0$ a vertical force is applied; then the boundary conditions at the free surface are of the form

$$(v_p^2-2v_s^2)\frac{\partial U}{\partial x}+v_p^2\frac{\partial W}{\partial z}\bigg|_{z=0}=F(x-x_0)f(t) \tag{83}$$

$$\frac{\partial W}{\partial x}+\frac{\partial U}{\partial z}\bigg|_{z=0}=0. \tag{84}$$

Here U and W are horizontal and vertical displacements, respectively. As earlier, we take $F(x-x_0)$ in the form

$$F(x-x_0)=\sqrt{\frac{n_0}{\pi}}e^{-n_0(x-x_0)^2}. \tag{85}$$

Having selected the parameter n_0 large enough, we will have a source which is close to a line force. The second-order partial differential equations, describing *P-SV*-wave propagation in a two-dimensional medium with Cartesian coordinates x and z can be written as

$$\frac{\partial}{\partial x}\left[v_p^2\frac{\partial U}{\partial x}+(v_p^2-2v_s^2)\frac{\partial W}{\partial z}\right]+\frac{\partial}{\partial z}\left[v_s^2\left(\frac{\partial W}{\partial x}+\frac{\partial U}{\partial z}\right)\right]=\frac{\partial^2 U}{\partial t^2}, \tag{86}$$

$$\frac{\partial}{\partial x}\left[v_s^2\left(\frac{\partial W}{\partial x}+\frac{\partial U}{\partial z}\right)\right]+\frac{\partial}{\partial z}\left[v_p^2\frac{\partial W}{\partial z}+(v_p^2-2v_s^2)\frac{\partial U}{\partial x}\right]=\frac{\partial^2 W}{\partial t^2} \tag{87}$$

with zero initial values

$$U|_{t=0}=W|_{t=0}=\frac{\partial U}{\partial t}\bigg|_{t=0}=\frac{\partial W}{\partial t}\bigg|_{t=0}=0. \tag{88}$$

Let us introduce the new boundary conditions

$$U|_{\substack{x=0\\x=b}}=0,\qquad \frac{\partial W}{\partial x}\bigg|_{\substack{x=0\\x=b}}=0. \tag{89}$$

We apply the cosine and sine integral transforms with finite limits to the system of Eqs. (86), (87):

$$R(z,n,t)=\int_0^b W(z,x,t)\cos\frac{n\pi x}{b}dx, \tag{90}$$

$$W(z,x,t)=\frac{1}{b}R(z,0,t)+\frac{2}{b}\sum_{n=1}^{\infty}R(z,n,t)\cos\frac{n\pi x}{b}, \tag{91}$$

$$S(z,n,t)=\int_0^b U(z,x,t)\sin\frac{n\pi x}{b}dx, \tag{92}$$

$$U(z,x,t)=\frac{2}{b}\sum_{n=1}^{\infty}S(z,n,t)\sin\frac{n\pi x}{b}. \tag{93}$$

We multiply Eq. (86) by $\sin\frac{n\pi x}{b}$ and Eq. (87) by $\cos\frac{n\pi x}{b}$ and integrate by parts from 0 to b, making use of conditions (89). Then substituting the series (91), (93) instead of $W(z,x,t)$ and $U(z,x,t)$ in the integral terms of the system obtained, we have:

$$\begin{aligned}
&\frac{\partial^2 S(z,n,t)}{\partial t^2}=-\frac{n\pi^2}{b^2}\sum_{m=0}^{\infty}m\cdot S(z,m,t)\\
&\cdot\frac{2}{b}\int_0^b v_p^2(x,z)\cos\frac{m\pi x}{b}\cos\frac{n\pi x}{b}dx\\
&-\frac{n\pi}{b}\sum_{m=0}^{\infty}\frac{\partial R(z,m,t)}{\partial z}\frac{2}{b}\int_0^b[v_p^2(x,z)-2v_s^2(x,z)]\\
&\cdot\cos\frac{m\pi x}{b}\cos\frac{n\pi x}{b}dx\\
&-\frac{\pi}{b}\sum_{m=0}^{\infty}m\cdot\frac{2}{b}\int_0^b\frac{\partial}{\partial z}[v_s^2(x,z)R(z,m,t)]\\
&\cdot\sin\frac{m\pi x}{b}\sin\frac{n\pi x}{b}dx\\
&+\sum_{m=1}^{\infty}\frac{2}{b}\int_0^b\frac{\partial}{\partial z}\left[v_s^2(x,z)\frac{\partial S(z,m,t)}{\partial z}\right]\sin\frac{m\pi x}{b}\sin\frac{n\pi x}{b}dx,
\end{aligned} \tag{94}$$

$$\begin{aligned}
&\frac{\partial^2 R(z,n,t)}{\partial t^2}=-\frac{n\pi^2}{b^2}\sum_{m=0}^{\infty}m\cdot R(z,m,t)\frac{2}{b}\int_0^b v_s^2(x,z)\\
&\cdot\sin\frac{m\pi x}{b}\sin\frac{n\pi x}{b}dx\\
&+\frac{n\pi}{b}\sum_{m=1}^{\infty}\frac{\partial S(z,m,t)}{\partial z}\frac{2}{b}\int_0^b v_s^2(x,z)\sin\frac{m\pi x}{b}\sin\frac{n\pi x}{b}dx\\
&+\sum_{m=0}^{\infty}\frac{2}{b}\int_0^b\frac{\partial}{\partial z}\left[v_p^2(x,z)\frac{\partial R(z,m,t)}{\partial z}\right]\cos\frac{m\pi x}{b}\cos\frac{n\pi x}{b}dx\\
&+\frac{\pi}{b}\sum_{m=1}^{\infty}m\cdot\frac{2}{b}\int_0^b\frac{\partial}{\partial z}[(v_p^2(x,z)-2v_s^2(x,z))S(z,m,t)]\\
&\cdot\cos\frac{m\pi x}{b}\cos\frac{n\pi x}{b}dx.
\end{aligned}$$

If we take the velocities v_p and v_s independent of the coordinate x very close to the free surface, the boundary conditions for $z=0$ will be as follows:

$$\begin{aligned}
&v_p^2\frac{\partial R(z,n,t)}{\partial z}+(v_p^2-2v_s^2)\frac{n\pi}{b}S(z,n,t)\big|_{z=0}\\
&=e^{-\frac{n^2\pi^2}{4b^2n_0}}\cos\frac{n\pi x_0}{b}f(t),
\end{aligned} \tag{96}$$

$$\frac{\partial S(z,n,t)}{\partial z}-\frac{n\pi}{b}R(z,n,t)\big|_{z=0}=0. \tag{97}$$

Problem (94)–(97) is solved with zero initial values

$$\begin{aligned}
S(z,n,t)|_{t=0}=R(z,n,t)|_{t=0}&=\frac{\partial S(z,n,t)}{\partial t}\bigg|_{t=0}\\
&=\frac{\partial R(z,n,t)}{\partial t}\bigg|_{t=0}=0.
\end{aligned} \tag{98}$$

Problem (94)–(98) is solved by means of an explicit finite difference scheme with a truncation error of second order. System (94), (95) degenerates into two equations with a parameter n, if the velocity is only a function of the coordinate z.

For some particular models of two-dimensional media one can obtain special one-dimensional equations with a shift parameter (Mikhailenko and Korneev, 1984).

The above approach requires less computer time than the second version of the algorithm and than the pseudospectral method. At the same time it allows us to calculate complete synthetic seismograms for Lamb's problem.

5.3. Calculation of complete theoretical seismograms for a three-dimensional half-space

In previous sections we discussed propagation of seismic waves from a line source in two-dimensional inhomogeneous media. However, for the comparison of theoretical seismograms with observed records, we should consider spherical waves, since amplitudes of reflected, diffracted and other waves, are not only affected by reflection coefficients, but also by spherical divergence.

Now we consider the propagation of P and SV waves in a medium which is axially symmetric and has complex subsurface geometry. Here, the velocities v_p and v_s are arbitrary functions of the two spatial variables r and z. The physical model selected can be described by the equations

$$\begin{aligned}
&\frac{\partial}{\partial r}\left(v_p^2\frac{\partial U_r}{\partial r}\right)+\frac{\partial}{\partial z}\left[v_s^2\left(\frac{\partial U_z}{\partial r}+\frac{\partial U_r}{\partial z}\right)\right]+\frac{\partial}{\partial r}\left[(v_p^2-2v_s^2)\frac{U_r}{r}\right]\\
&\qquad+\frac{\partial}{\partial r}\left[(v_p^2-2v_s^2)\frac{\partial U_z}{\partial z}\right]+2v_s^2\frac{\partial}{\partial r}\left(\frac{U_r}{r}\right)=\frac{\partial^2 U_r}{\partial t^2},
\end{aligned} \tag{99}$$

$$\begin{aligned}
&\frac{\partial}{\partial r}\left(v_s^2\frac{\partial U_r}{\partial r}\right)+\frac{\partial}{\partial z}\left[(v_p^2-2v_s^2)\left(\frac{\partial U_r}{\partial r}+\frac{U_r}{r}\right)+v_p^2\frac{\partial U_z}{\partial z}\right]\\
&\qquad+\frac{\partial}{\partial r}\left[v_s^2\frac{\partial U_r}{\partial z}\right]+v_s^2\frac{1}{r}\frac{\partial U_r}{\partial z}+v_s^2\frac{1}{r}\frac{\partial U_z}{\partial r}=\frac{\partial^2 U_z}{\partial t^2}.
\end{aligned} \tag{100}$$

Let us assume that the medium consists of two regions as shown in Fig. 10. Medium 2 is located at some distance from $r=0$. Medium 2 is assumed to be two-dimensionally inhomogeneous, and the propagation of seismic waves in it is described by system (99) and

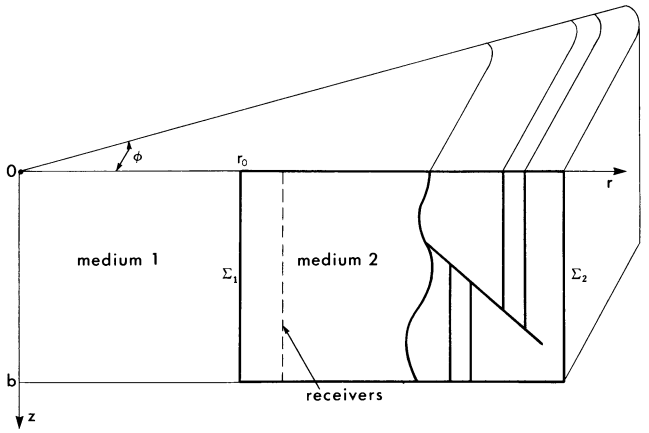

Fig. 10. Geometry of the medium considered. The medium is assumed to be radially symmetric in the cylindrical system of coordinates (r, φ, z) indicated in the figure. The source is located in medium 1, which is isotropic and homogeneous. The source may lie at any point along the z axis between 0 and b. Medium 2 is a generally inhomogeneous medium, and it is in this medium where the receivers are located

(100). We choose the line of receivers to be located in this region. It is assumed that the medium in region 1 is an isotropic homogeneous medium. If the receivers are located in region 2 far removed from the source we may neglect the effect of three-dimensional curved boundaries. The problem is in effect three-dimensional, but it can be formulated in terms of a problem in two dimensions because the medium varies only in two coordinates, r and z.

As the medium in region 1 is isotropic and homogeneous, an analytic solution for the system of Eqs. (99), (100) can be obtained and connected across the boundary Σ_1 to medium 2 where a numerical solution must be formulated. This problem will be discussed later.

According to the first version of our algorithm we apply the finite integral Fourier transform and the finite difference technique for the numerical solution of system (99), (100) in region 2. The boundary conditions for $z=0$ and $z=b$ are:

$$\left.\frac{\partial U_r}{\partial z}\right|_{\substack{z=0\\z=b}} = 0, \qquad U_z|_{\substack{z=0\\z=b}} = 0. \tag{101}$$

As the source is located in an isotropic homogeneous medium, an analytic solution for an explosive-type point source may be presumed with initial conditions of the form

$$U_z|_{t=0} = U_r|_{t=0} = \left.\frac{\partial U_z}{\partial t}\right|_{t=0} = \left.\frac{\partial U_r}{\partial t}\right|_{t=0} = 0. \tag{102}$$

The initial conditions in medium 2 are obtained by matching the analytic solution in medium 1 to the numerical solution across the interface Σ_1.

We will now introduce finite sine and cosine transforms and their inverses which we will use in reducing the dimensionality of Eqs. (99) and (100):

$$R(r,n,t) = \int_0^b U_z \sin\frac{n\pi z}{b}\,dz, \tag{103}$$

$$U_z(r,z,t) = \frac{2}{b}\sum_{n=1}^{\infty} R(r,n,t)\sin\frac{n\pi z}{b}, \tag{104}$$

$$S(r,n,t) = \int_0^b U_r \cos\frac{n\pi z}{b}\,dz, \tag{105}$$

$$U_r(r,z,t) = \frac{1}{b}S(r,0,t) + \frac{2}{b}\sum_{n=1}^{\infty} S(r,n,t)\cos\frac{n\pi z}{b}. \tag{106}$$

As earlier, we will employ these finite transforms so that the unknown quantities become $R(r,n,t)$ and $S(r,n,t)$ instead of $U_r(r,z,t)$ and $U_z(r,z,t)$. The obtained system of partial differential equations may be presented in the following finite difference form:

$$\frac{1}{\Delta t^2}\{S_k^{j+1}(n) - 2S_k^j(n) + S_k^{j-1}(n)\}$$
$$= \sum_{m=0}^{\infty}\{A_k^j(m)\,C_{k+1}(m,n) + B_k^j(m)\,C_k(m,n)$$
$$+ E_k^j(m)\,C_{k-1}(m,n) + H_k^j(m)\,F_k(m,n)\}, \tag{107}$$

$$\frac{1}{\Delta t^2}\{R_k^{j+1}(n) - 2R_k^j(n) + R_k^{j-1}(n)\} = \sum_{m=0}^{\infty}\{P_k^j(m)\cdot F_{k+1}(m,n)$$
$$+ Q_k^j(m)\,F_k(m,n) + T_k^j(m)\,F_{k-1}(m,n) - V_k^j(m)\,C_k(m,n), \tag{108}$$

where

$$C_k(m,n) = \frac{2}{b}\int_0^b V_{pk}^2(z)\cos\frac{m\pi z}{b}\cos\frac{n\pi z}{b}\,dz$$
$$= [D_k(m+n) + D_k(m-n)], \tag{109}$$

$$F_k(m,n) = \frac{2}{b}\int_0^b V_{pk}^2(z)\sin\frac{m\pi z}{b}\sin\frac{n\pi z}{b}\,dz$$
$$= [D_k(m-n) - D_k(m+n)], \tag{110}$$

$$D_k(m\pm n) = \frac{1}{b}\int_0^b V_{pk}^2(z)\cos\frac{(m\pm n)\pi z}{b}\,dz, \tag{111}$$

and A_k^j, B_k^j, E_k^j, H_k^j, P_k^j, Q_k^j, T_k^j and V_k^j are known functions. For more details see Mikhailenko (1984).

If the velocity depends only on the spatial coordinate r we arrive at a system of equations of the form

$$\frac{\partial}{\partial r}\left[V_p^2\frac{\partial S}{\partial r}\right] + \frac{\partial}{\partial r}\left[(V_p^2 - 2V_s^2)\frac{S}{r}\right]$$
$$+ 2V_s^2\frac{\partial}{\partial r}\left[\frac{S}{r}\right] - \left(V_s\frac{n\pi}{b}\right)^2 S$$
$$+ V_s^2\frac{n\pi}{b}\frac{\partial R}{\partial r} + \frac{n\pi}{b}\frac{\partial}{\partial r}\left[(V_p^2 - 2V_s^2)R\right] = \frac{\partial^2 S}{\partial t^2}, \tag{112}$$

$$\frac{\partial}{\partial r}\left[V_s^2\frac{\partial R}{\partial r}\right] + V_s^2\frac{1}{r}\frac{\partial R}{\partial r} - \left(V_p\frac{n\pi}{b}\right)^2 R - \frac{n\pi}{b}\frac{\partial}{\partial r}(V_s^2 S)$$
$$- \frac{n\pi}{b}(V_p^2 - 2V_s^2)\frac{\partial S}{\partial r} - \frac{n\pi}{b}(V_p^2 - V_s^2)\frac{S}{r} = \frac{\partial^2 R}{\partial t^2}. \tag{113}$$

Analytical solution for P, SV waves in a homogeneous medium. Let us consider an explosive-type point source which is located at some arbitrary depth along the z coordinate. We assume that $f(t)$ has the following form:

$$f(t) = \exp\{-[2\pi f_0(t-t_0)]^2/\gamma^2\}\sin[2\pi f_0(t-t_0)], \tag{114}$$

where f_0 is the predominant frequency, γ is a damping factor, and t_0 is selected such that $f(0) \approx 0$. In this case we can obtain an analytical solution as a series

$$R = -\left(\frac{n\pi}{b}\right) \cdot a(n, z_0) \sum_{i=1}^{\infty} \cos[\gamma(t-t_0)]\, b(v)\, c(k_i r_0), \qquad (115)$$

$$S = a(n, z_0) \sum_{i=1}^{\infty} \cos[\gamma(t-t_0)]\, b(v)\, d(k_i r_0), \qquad (116)$$

where the coefficients $a(n, z_0)$, $c(k_i r_0)$, $d(k_i r)\, b(v)$ are defined as follows:

$$a(n, z_0) = e^{-\frac{n^2\pi^2}{4b^2 n_0}} \cos\frac{n\pi z_0}{b},$$

$$c(k_i r_0) = J_0(k_i r_0)/[J_1(k_i a)]^2,$$

$$d(k_i r_0) = -k_i J_1(k_i r_0)/[J_1(k_i a)]^2,$$

$$b(v) = \frac{1}{v}\{e^{-\left(\frac{(2\pi - v)^2}{\frac{4\pi f_0}{v}}\right)} - e^{-\left(\frac{(2\pi + v)^2}{\frac{2\pi f_0}{v}}\right)}\}, \qquad v = V_s \sqrt{\left(\frac{n\pi}{b}\right)^2 + k_i^2}.$$

Derivation of formulas (114) and (115) can be found in Mikhailenko (1984). With the help of these formulas we calculate the values of the functions $R(r, n, t)$ and $S(r, n, t)$ $(n = 0, 1, 2, 3, \ldots)$ at the point r_0, which is the first point of the finite difference Eqs. (107) and (108).

We have selected the explosive-type point source, although it is not difficult to obtain an analytical solution for other types of sources. Plane waves are also popular in problems of seismic exploration. It is not difficult to model a plane wave with the help of the analytical solution (114) and (115). In this case the values of functions $R(r, n, t)$ and $S(r, n, t)$ are nonzero for the harmonic $n = 0$ only. However, for the numerical solution in medium 2 we must use the same number of harmonics as for a point source. This can be seen from Eqs. (107) and (108), as in this case the solution is not equal to 0 for the harmonics $n = 1, \ldots, M$. Physically, this means that the secondary sources, i.e., the points in the laterally inhomogeneous medium, produce spherical waves which may be approximated only by a summation over a number of plane waves which means that many harmonics must be used. For numerical calculation we will use both plane waves and point sources.

Introduction of an absorbing boundary. In order to eliminate reflections from the pseudoboundary we must introduce an absorbing boundary condition. For this purpose, we make use of the results obtained by Clayton and Engquist (1977), where a parabolic approximation to the hyperbolic two-dimensional equations is introduced. Let us assume that in the vicinity of this pseudoboundary all velocities are constant. In this case we may obtain a system of one-dimensional equations for the function $R(r, n, t)$ and $S(r, n, t)$ for a fixed value of the parameter n. This system is of the form

$$\frac{\partial^2 S}{\partial r\, \partial t} + \frac{1}{V_p^2}\frac{\partial^2 S}{\partial t^2} + \frac{(V_s - V_p)}{V_p}\frac{n\pi}{b}\frac{\partial R}{\partial t} - \frac{(V_p - 2V_s)}{2}\left(\frac{n\pi}{b}\right)^2 S = 0, \qquad (117)$$

$$\frac{\partial^2 R}{\partial r\, \partial t} + \frac{1}{V_s^2}\frac{\partial^2 R}{\partial t^2} - \frac{(V_s - V_p)}{V_s}\frac{n\pi}{b}\frac{\partial S}{\partial t} - \frac{(V_s - 2V_p)}{2}\left(\frac{n\pi}{b}\right)^2 R = 0. \qquad (118)$$

This system is then formulated in finite difference form at the boundary Σ_2 (Mikhailenko, 1984).

Also, it should be noted that the boundaries at $z = 0$ and $z = b$ are reflective, too. In order to eliminate these reflections, it is necessary to select them far enough from the centre of the geological structure. Besides, it is possible to solve the problems twice, first with the boundary conditions

$$\left.\frac{\partial U_r}{\partial z}\right|_{\substack{z=0 \\ z=b}} = 0, \qquad U_z|_{\substack{z=0 \\ z=b}} = 0 \qquad (119)$$

and then with the alternative conditions

$$U_r|_{\substack{z=0 \\ z=b}} = 0, \qquad \left.\frac{\partial U_z}{\partial z}\right|_{\substack{z=0 \\ z=b}} = 0. \qquad (120)$$

After that the results are summed up.

It should be noted that for seismological problems instead of an absorbing boundary Σ_2 we introduce boundary conditions at the free surface $r = a$.

Comments on the Convergence and Accuracy of the Method. Here we will only mention the main factors affecting the convergence. For more details see Mikhailenko and Korneev (1984) and Mikhailenko (1984). Most important is the smoothness of the Fourier spectrum of $f(t)$, since we select the number of spatial harmonics in series (104) and (106) according to the highest temporal frequency in the spectrum of the source signal $f(t)$ and according to the minimal velocity of the medium. The number of harmonics in series (104) and (106) increases linearly with the increase of the distance $z = b$ to the reflecting surface. Here we take two harmonics per minimal wavelength.

An additional factor affecting the convergence of convolution sums of the type (75) is the decrease of coefficients $h_k(s)$ with increasing s. The convergence of these coefficients is directly related to the smoothness of the velocity in the medium, as follows from Eq. (73) for $s \to \infty$. In numerical calculations we approximate $v_{sk}(x)$ by a linear function on a uniform interval. In this case the convergence is as $1/s^2$ in Eq. (73). We may improve the convergence by approximating $v_{sk}(x)$ by spline functions of different orders in nonuniform intervals. Here the coefficients $h_k(s)$ are analytically calculated (Mikhailenko and Korneev, 1984).

In the numerical solution for medium 2, the time step is determined approximately by the following relations:

$$\left[\left(\frac{\Delta t}{\Delta r}\right)^2 + \left(\frac{n\pi\, \Delta t}{2b}\right)^2\right](V_p^2 + V_s^2) < 1. \qquad (121)$$

In practice, in our calculations we made use of the simple criterion

$$\frac{\Delta t \cdot V_{\max}}{\Delta r} \leqq 0.87. \qquad (122)$$

The total error of the method consists of the truncation error resulting from finite-difference schemes and the error from limiting the spatial frequencies in the Fourier series. The method was tested against several problems for particular models of inhomogeneous media calculated by the integral equations method (Vo-

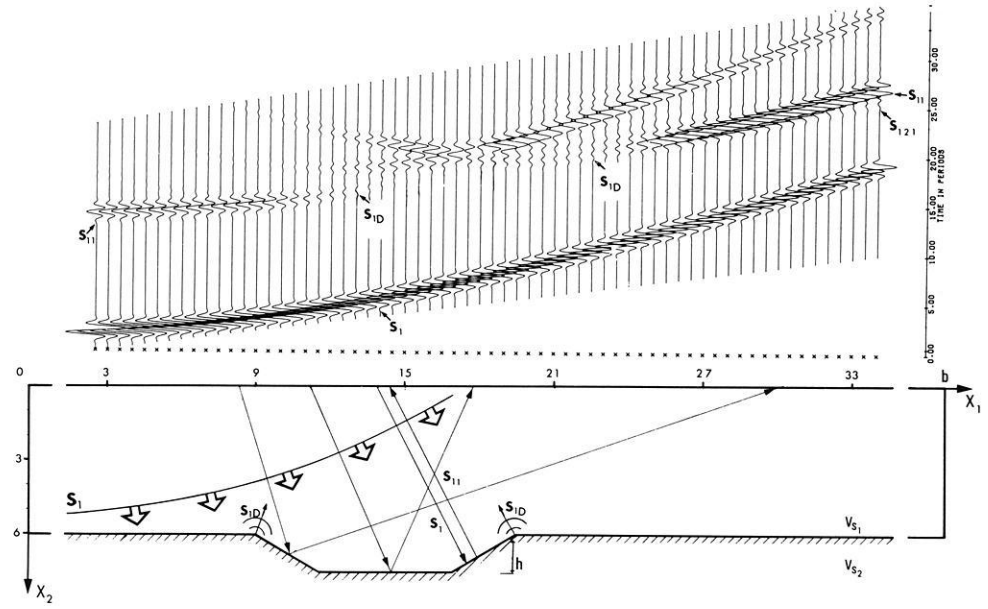

Fig. 11. Geometry of the medium and theoretical seismograms for SH waves ($x_1 = z, x_2 = r = 30\,WL$). The point source generating a spherical SH wave is located on the z axis at the point $r=0$, $z=0$. The velocity below the interface is twice that of the medium above it

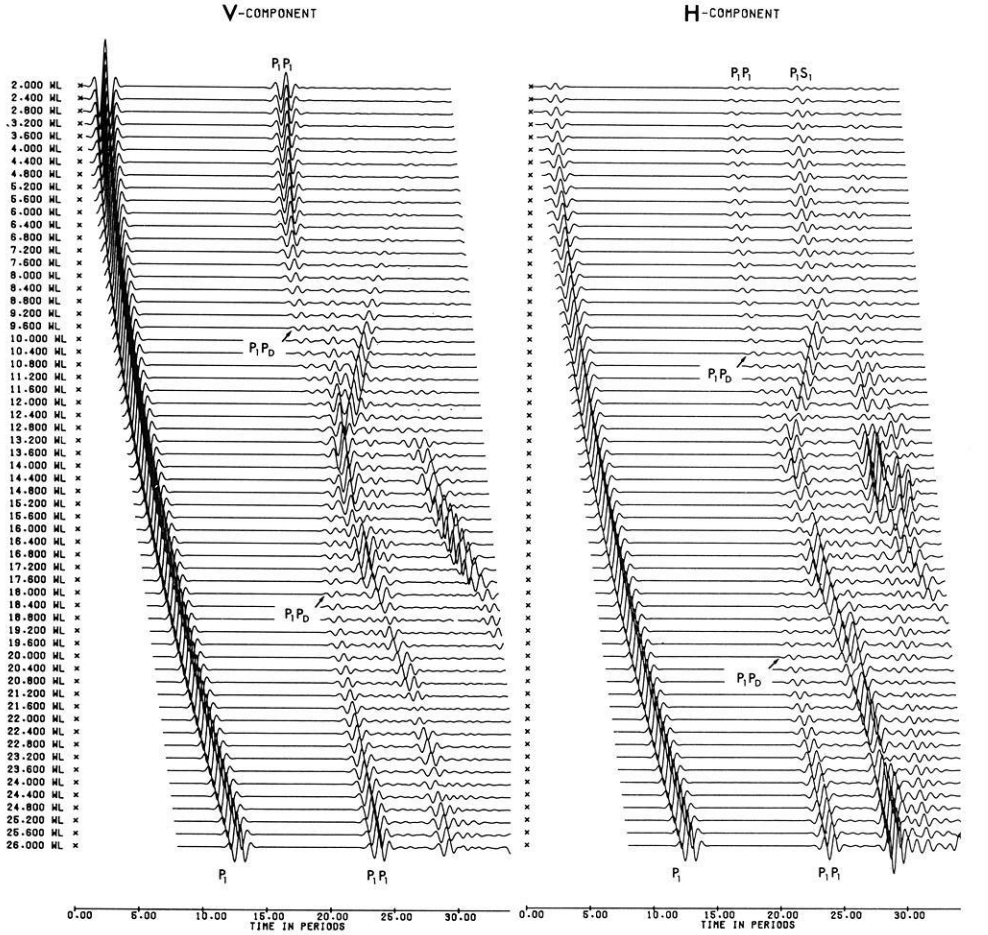

Fig. 12. Theoretical seismograms of the horizontal and vertical components of displacement for the medium shown in Fig. 11. An explosive-type point source is located on the z axis at the point $r=0$, $z=0$, $V_{p_2} = 2 \cdot V_{p_1}$, $V_{s_2} = 2 V_{s_1}$

ronin, 1978). The results obtained using the algorithms described here are in satisfactory agreement.

5.4. Examples of theoretical seismograms for media with complex geometries

The two versions of the algorithm discussed in this lecture make it possible to calculate seismograms for realistic subsurface geometries. However, we will not consider here a realistic complex model because its seismograms are difficult to understand. In this section we will present only the simplest geological models. In order to increase the range of applicability of our results, distance and time are expressed in terms of wavelengths (WL) and periods (T), respectively.

The time dependence of the source pulse used is

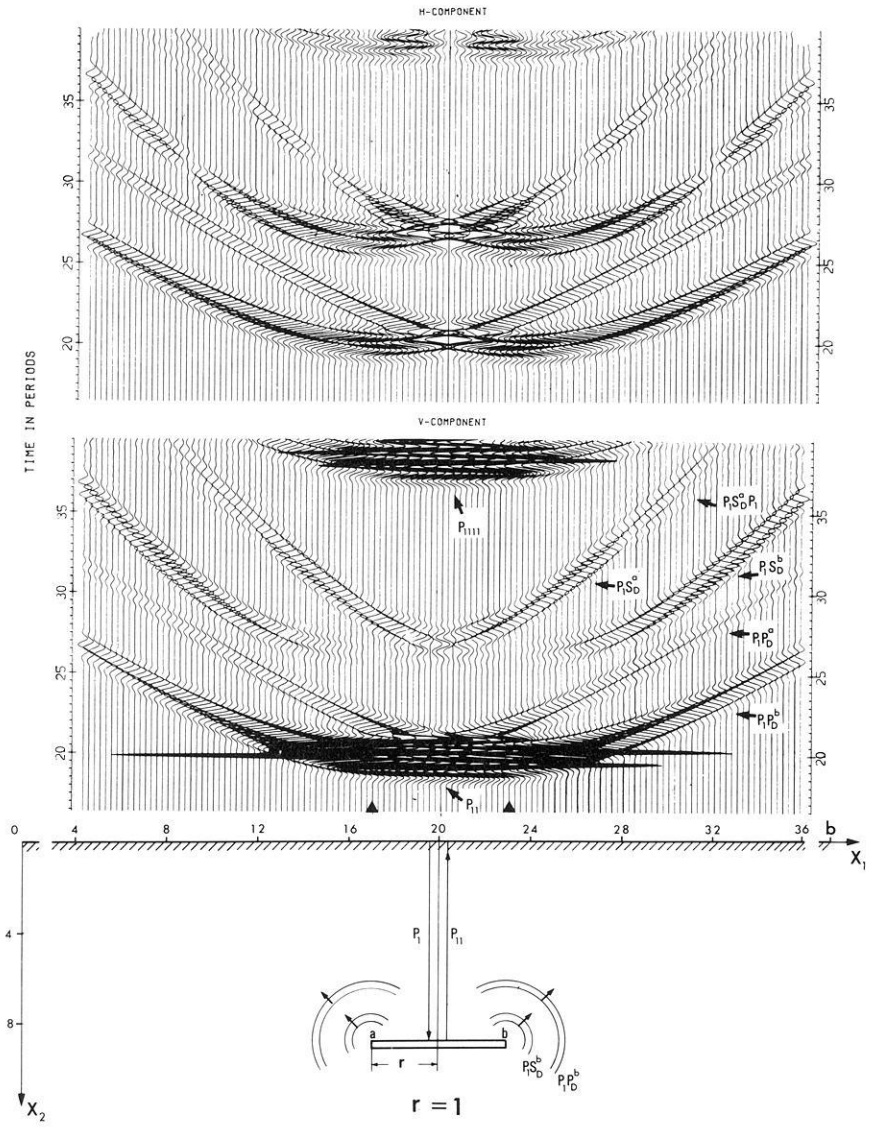

Fig. 13. Theoretical seismograms of the vertical and horizontal components of displacement generated by a plane P wave for a model medium consisting of a high-velocity inclusion whose radius r is equal to one Fresnel zone. The velocity of P and S waves in the inclusion is twice the one outside it ($V_S/V_P=0.6$). The inclusion thickness is $h=0.25\,WL$

given by formula (114). Here we will consider only sources generating either P or SH waves, although the algorithm for the calculation of SH waves in complex subsurface structures with radial symmetry was not discussed here (Mikhailenko, 1984). In our calculation we will use also a plane wavefront which is convenient in the interpretation of theoretical seismograms.

Let us consider the case of a symmetric basin. Figure 11 shows this model and theoretical seismograms. The receivers are located close to the surface Σ_1, which is $30\,WL$ away from the axis $0z$. The point source generating a spherical SH wave is located on the z axis at the point $r=0$, $z=0$. In the figure the front of the wave incident from the source is denoted by S_1, x_1 and x_2 denote the coordinates z and $r=30\,WL$, respectively. The velocity below the interface is twice that of the medium above it. The quantity $h=1.5\,WL$. The identification of arrivals is as follows: S_1 – direct arrival, S_{11} – reflected arrival, S_{1D} – diffracted arrival. The distance between the receivers is $0.5\,WL$.

A more complicated picture may be observed if a spherical P wave is incident on the same structure. In this case, besides PP waves, there are converted PS waves. Theoretical seismograms for the vertical and horizontal displacement components are presented in Fig. 12.

As is seen, the wave picture is far from being simple. To simplify the interpretation of seismograms, we found it appropriate to change from the spherical wave to a plane wave. This plane wave may be constructed by means of a set of point sources. In Fig. 13 we see the diffraction of a vertically incident plane P wave by a high velocity elastic inclusion. Note that the direct P wave is cut off in all the figures. The inclusion is located at a distance of $9\,WL$ from the free surface. The size of the inclusion equals $6\,WL$ which corresponds to the radius r of the first Fresnel zone. The velocity of longitudinal and shear waves in the inclusion is twice the velocity outside, and the ratio $V_s/V_p=0.6$. At the edges a and b of the inclusion diffracted P and S waves are generated. Since the wave picture is symmetrical with respect to the centre of the inclusion, we will consider the diffraction tails of P waves and the two diffraction tails of S waves from the edges a and b. The diffraction

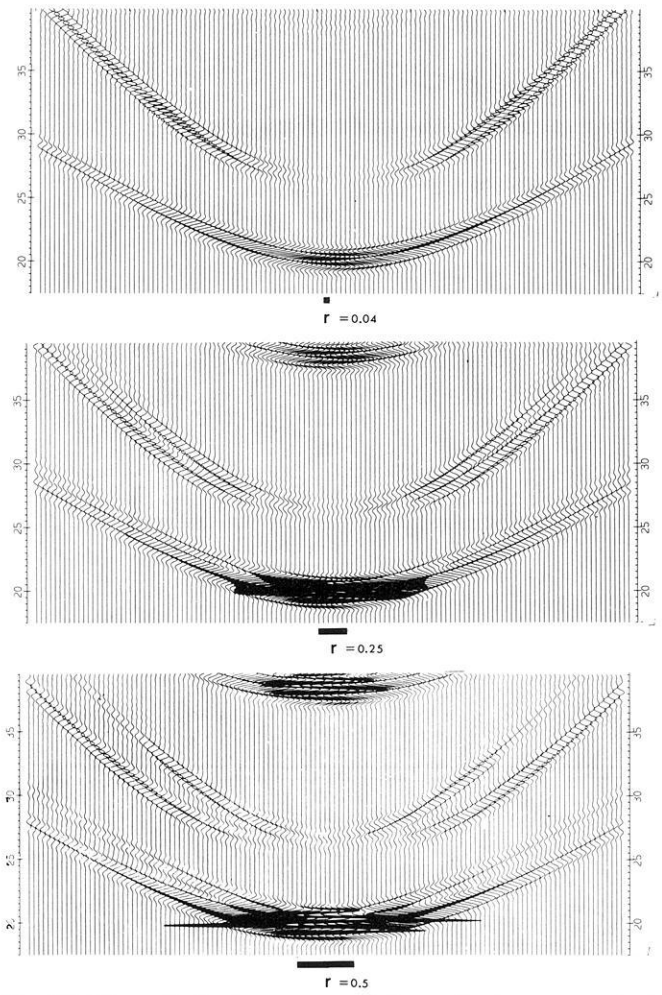

Fig. 14. Theoretical seismograms of the vertical component of displacement for the model medium shown in Fig. 13. The width of the inclusion is selected as follows: (a) 0.5 of the Fresnel zone, (b) 0.25 of the Fresnel zone, (c) 0.04 of the Fresnel zone

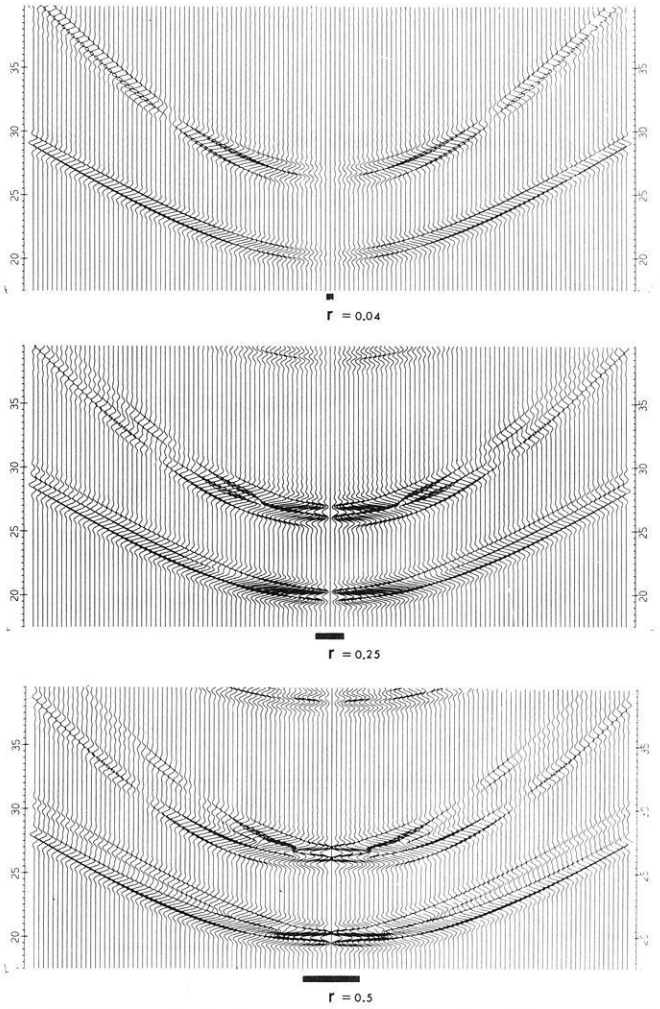

Fig. 15. Theoretical seismograms of the horizontal component of displacement for the model medium shown in Fig. 13. The width of the inclusion is as follows: (a) 0.5 of the Fresnel zone, (b) 0.25 of the Fresnel zone, (c) 0.04 of the Fresnel zone

tail of the P wave from point b has the same polarity as the reflection event, while the diffraction tail from point a has polarity opposite to the reflection event. This is a well-known fact. A similar situation takes place also for diffraction tails of S waves. However, if the diffracted S wave is incident on the free surface under the angle $\alpha = \arcsin(V_s/V_p)$ a longitudinal head wave $P_1 S_D P_1$ is generated. Besides, linear polarization of the diffracted shear wave $P_1 S_D$ changes to elliptic polarization. As is seen in Fig. 13 the horizontal displacement component passes through zero. The amplitudes of waves reflected by the inclusion are zero on the horizontal component because we use a plane wave. We should note that the amplitude of the reflected P wave is reduced to 50% directly above the edges of the inclusion.

With decreasing size of the inclusion the wave picture becomes closer to the wave picture obtained with a point diffractor. We can see this in Figs 14 and 15, where vertical and horizontal displacement components are presented. All the parameters of the previous model stay the same here except for the size of the inclusion. As we can judge from the calculations, diffracted (or scattered) S waves have the same amplitude as P waves, even when the size of the inclusion is small.

Although in this section we deal with two-dimensional models, the divergence is the same as in a three-dimensional case, if receivers are located not far from structures.

Let us now consider simple two-dimensional reef models. To simplify interpretation of theoretical seismograms, we will use a vertically incident plane SH wave. Figure 16 shows the theoretical seismograms for a reef (model A), for a reef with smoothed upper edges (model B) and for a salt dome (model C). The main wave types are marked in model A. Since the wave picture is symmetrical with respect to the centre of the reef, we show only parts of the profiles on the left.

Interference of diffracted waves from the zone of inflection of the geological horizon gives a false impression of its continuity beneath the reef. Besides, as we see from the figure, there is an intense wave which arrives after the S_{11} wave reflected from the horizon. In order to understand its origin let us consider models B

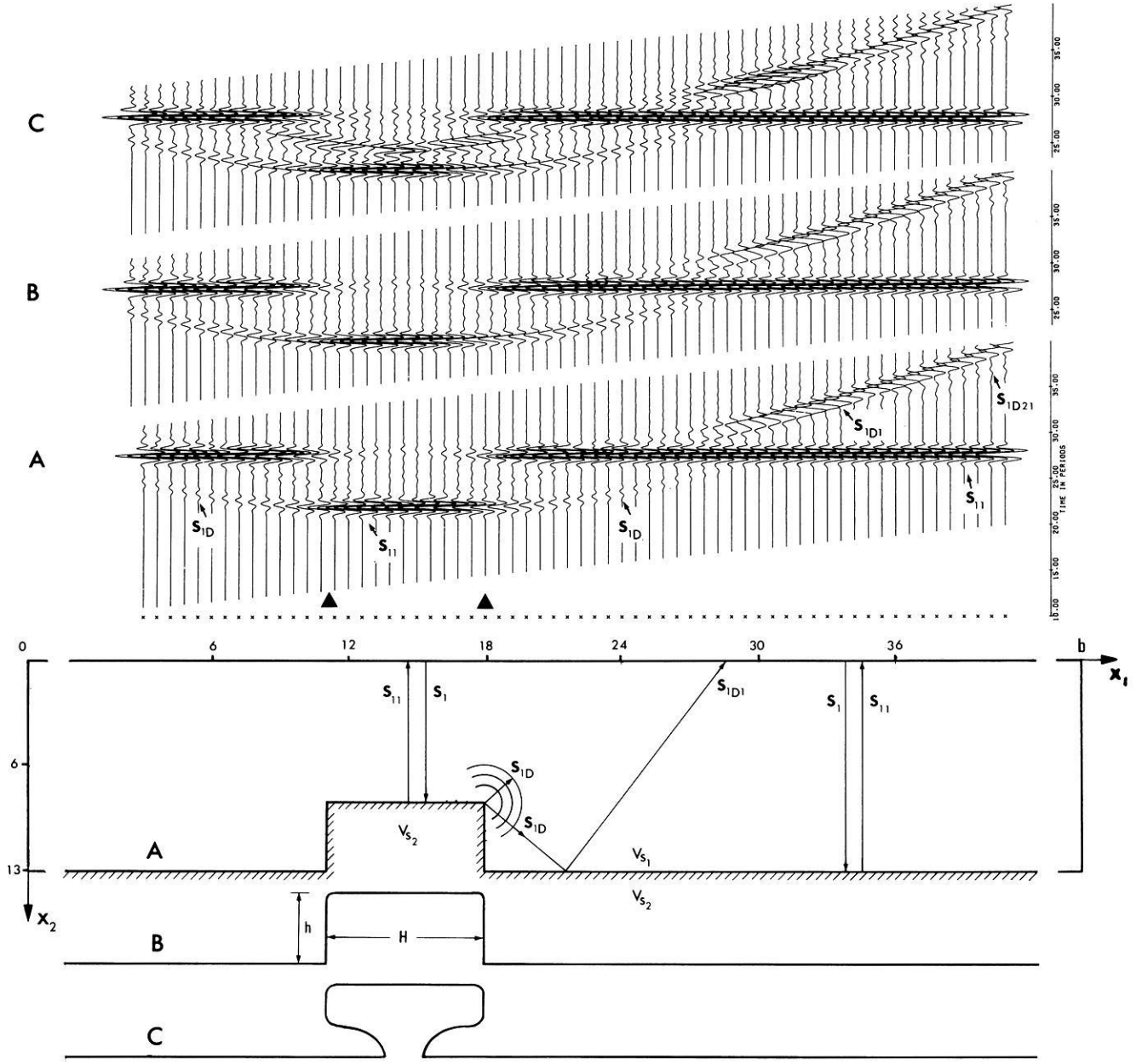

Fig. 16. Theoretical seismograms for an *SH*-plane wave normally incident on the three structures A, B, C. The *S* velocity inside the structures is twice that above them

and C. As is seen, the smoothed upper edges of the reef produce more intense diffracted (scattered) S_{1D} waves. Variation in the location of the lower reef edges does not cause any change in arrival time of the above-mentioned intense wave.

Let us consider the three models and theoretical seismograms shown in Fig. 17. Model C and its corresponding seismograms are taken from the previous figure. Model D is constructed as follows: We take the upper part of model C and make the geologic horizon continuous. Thus, we obtain some high velocity inclusion above the geologic horizon. Model F represents the above inclusion without geologic horizon.

The analysis of these models leads to the conclusion that the intense wave which arrives after the reflected S_{11} wave is a diffracted (scattered)-reflected wave. The diffracted (scattered) wave from the upper part of the salt dome is incident under the critical angle on the geologic horizon. The wave reflected from this horizon generates a head wave S_{1D21}.

We now consider the model and theoretical seismograms presented in Fig. 18. The plane *SH* wave is normally incident on a half-infinite high-velocity layer of thickness $0.25\,WL$ ($V_{S_2}=2V_{S_1}$). Here one can also see a diffracted-reflected wave which arises each time multiple reflections from the horizon and the free surface are incident on the edge of the layer.

When the distance d between the layer and the horizon decreases the wave picture becomes more complicated. The diffracted wave and the diffracted-reflected wave interfere. This can be seen in Fig. 19.

We next consider a two-dimensional monocline

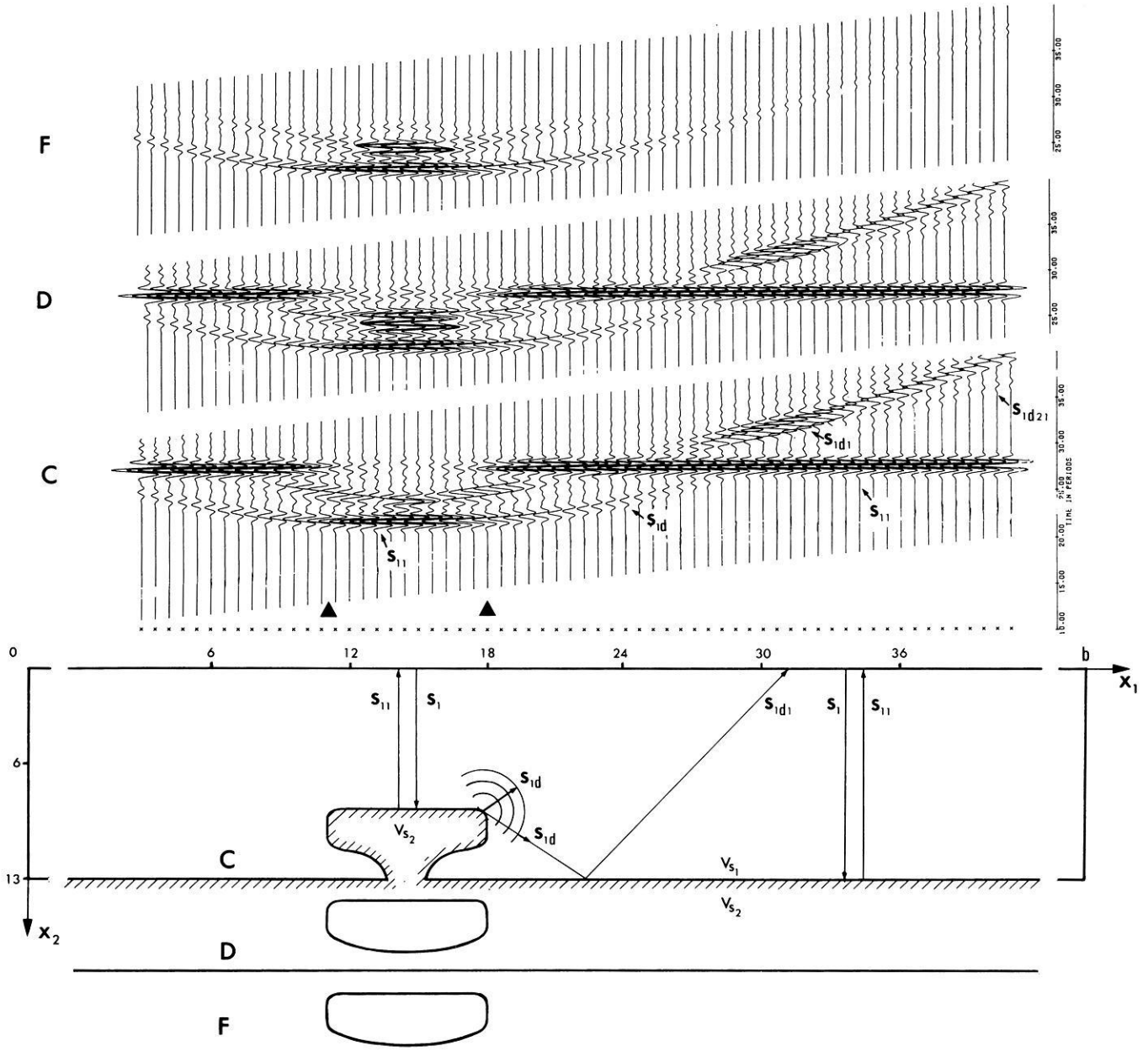

Fig. 17. Theoretical seismograms for an *SH*-plane wave normally incident on the three structures C, D, F. The *S* velocity inside the structures is twice that above them

model. The plane connecting the two half-planes has a dip of 45°. The velocity below these planes is twice the velocity above them. If the *SH* wave is normally incident, the reflected waves from the dipping plane propagate in the horizontal direction and do not come to the receivers. However, we observe on the theoretical seismograms a relatively intense diffracted-reflected wave and head waves (Fig. 20).

Thus, from numerical experiments it becomes clear that diffracted-reflected and diffracted head waves can be rather intense, and that they may possibly be used in seismic exploration. I would like to propose an approach which is based on the cancellation of multiple waves and on the investigation of diffracted waves. The idea is to use plane *P* waves and recordings of the horizontal component of the displacement vector. Let there be some inclusion or stratigraphic trap inside the stratified medium. If we construct a plane wave with the help of point sources, the amplitudes of all multiply reflected waves on the horizontal displacement component will be zero. In this case we will have only diffracted waves, if the medium changes only in the vertical direction. This is illustrated in Fig. 21, where a plane *P* wave is incident on a flat layered medium containing an inclusion. The parameters used are $V_{p_3} = 2V_{p_1}$, $V_{s_3} = 2V_{s_1}$, $V_s/V_p = 0.6$, $V_{p_2} = 1.5\,V_{p_1}$, $V_{s_2} = 1.5\,V_{s_1}$. The thickness of the inclusion is 0.25 *WL*. Note that the direct *P* wave is cut off in the figure. As is seen in the figure, multiply reflected waves are absent on the horizontal component, and we have only diffracted waves. It is easy to determine the location of the middle part of the inclusion where the horizontal component equals

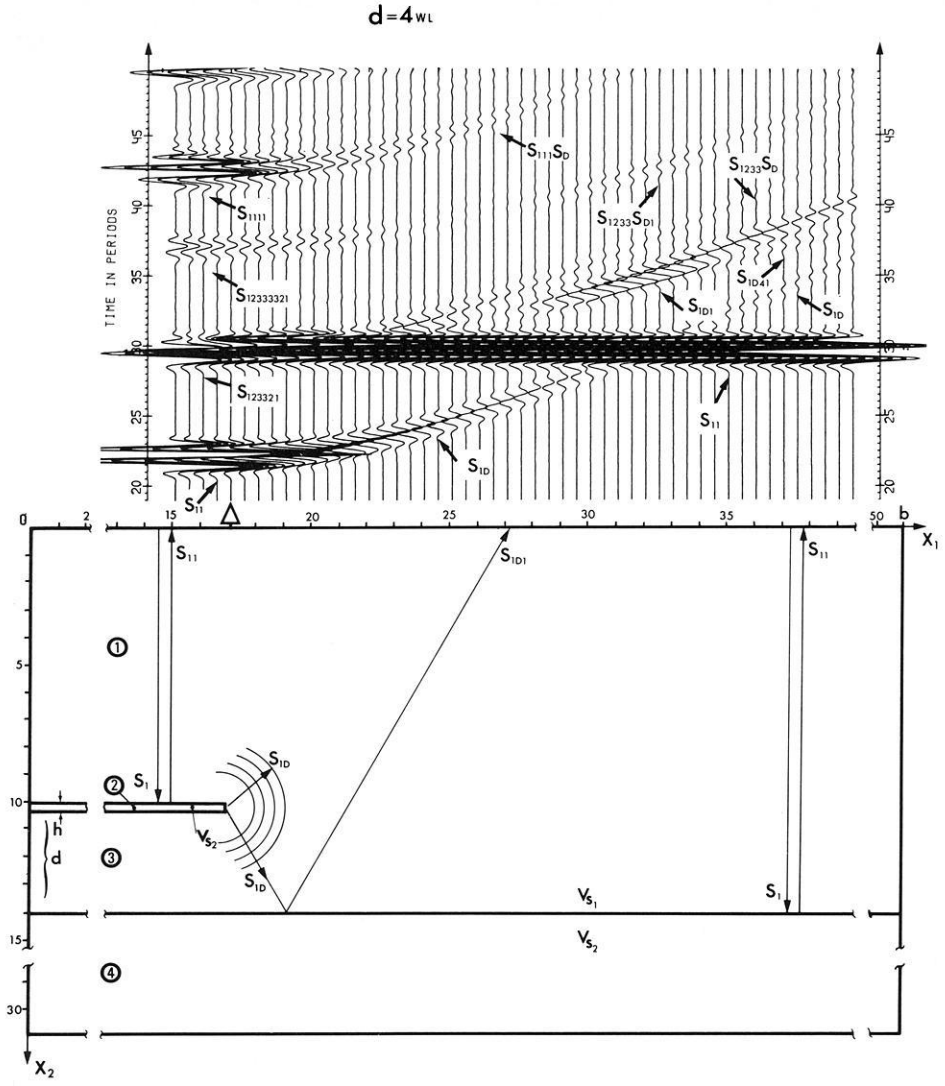

Fig. 18. Theoretical seismograms for an *SH*-plane wave normally incident in a half-infinite high-velocity layer. The thickness of the layer is 0.25 *WL*, $d = 4\,WL$ ($V_{S_2} = 2V_{S_1}$)

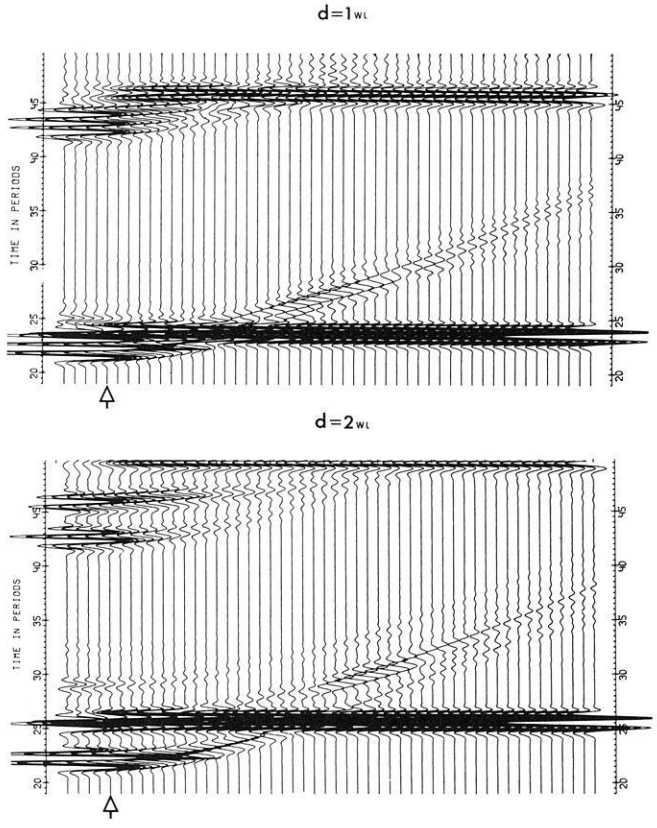

Fig. 19. Theoretical seismograms for an *SH*-plane wave normally incident on a half-infinite high-velocity layer. The thickness of the layer is 0.25 *WL*, ($V_{S_2} = 2V_{S_1}$). *Bottom:* $d = 2\,WL$. *Top:* $d = 1\,WL$

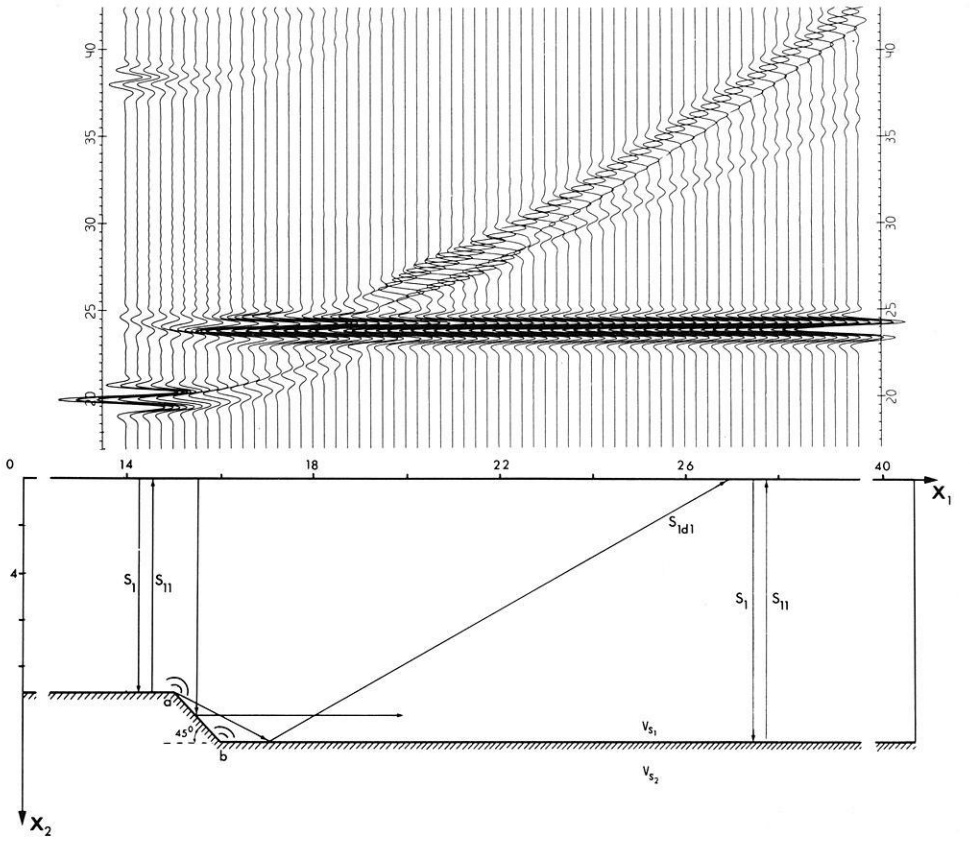

Fig. 20. Theoretical seismograms for an *SH*-plane wave normally incident on a two-dimensional monocline model which has a dip of 45°. The velocity inside the structure is twice that above it

zero. At present work has begun on implementation of this approach in seismic exploration.

Conclusion

We have considered and discussed the main stages of numerical experiments in seismic exploration for one- and two-dimensional inhomogeneous models of media. The approach presented is being developed for the calculation of complete theoretical seismograms and for three-dimensional inhomogeneous media. In this case two-dimensional Fourier transform along the coordinates x and y and the finite difference technique along the coordinate z is used. Here we introduce an absorbing condition at the boundary $z=z_0$. Note that for the calculation of three-dimensional models of realistic media it is necessary to use high performance computers.

References

Alekseev, A.S., Mikhailenko, B.G.: Solution of Lamb's problem for a vertically inhomogeneous half-space (in Russian). Izv. Akad. Nauk SSSR, Fizika Zemli **12**, 11–25, 1976

Alekseev, A.S., Mikhailenko, B.G.: Method of calculation of theoretical seismograms for complex models of media (in Russian). Dokl. Akad. Nauk SSSR **240**, 1062–1065, 1978

Alekseev, A.S., Mikhailenko, B.G.: Solution of dynamic problems of elastic wave propagation in inhomogeneous media by a combination of partial separation in variables and finite difference methods. J. Geophys. **48**, 161–172, 1980

Clayton, R., Engquist, B.: Absorbing boundary conditions for acoustic and elastic wave equations. Bull. Seismol. Soc. Amer. **67**, (6), 1529–1540, 1977

Coussy, O., Bourbie, T.: Propagation des ondes acoustiques dans les milieux poreux saturés. Rev. Inst. fr. pétrole, **39**, No. 1, 47–66, 1984

Crampin, S.: A review of wave motion in anisotropic and cracked elastic media. Wave motion **3**, 433–491, 1981

Deriagin, B.V.: Zhurnal geofiziki (in Russian), No. 1, 2, 207, 1931

Fatianov, A.G., Mikhailenko, B.G.: Numerical solution of Lamb's problem for nonelastic inhomogeneous Boltzmann's medium with elastic aftereffect (in Russian). Matematicheskie metody interpretacii geofizicheskikh nabljudenijj. Novosibirsk, 115–160, 1979

Fatianov, A.G.: Numerical solution of Lamb's problem for non-elastic inhomogeneous Boltzmann's half-space (in Russian). Chislennye metody i interpreticija geofizicheskikh nabljudenijj. Novosibirsk, 144–156, 1980

Fatianov, A.G., Mikhailenko, B.G.: Non-stationary seismic wave fields in inhomogeneous visco-elastic model media (in Russian). Matematicheskije problemy geofiziki: modeli i chislennye metody 70–120, Novosibirsk, 1984

Gazdag, J.: Numerical convective schemes based on the accurate computation of space derivatives. J. Comput. Phys. **13**, 100–113, 1973

Gazdag, J.: Modeling of the acoustic wave equation with transform methods. Geophysics **46**, 854–859, 1981

Kosloff, D., Baysal, E.: Forward modeling by a Fourier method. Geophysics **47**, 1402–1412, 1982

Kreis, H.O., Oliger, J.: Comparison of accurate methods for the integration of hyperbolic equations. Tellus **24**, 199–215, 1972

Martynov, V.N., Mikhailenko, B.G.: Numerical modelling of propagation of elastic waves in anisotropic inhomogeneous media for the half-space and the sphere (in Rus-

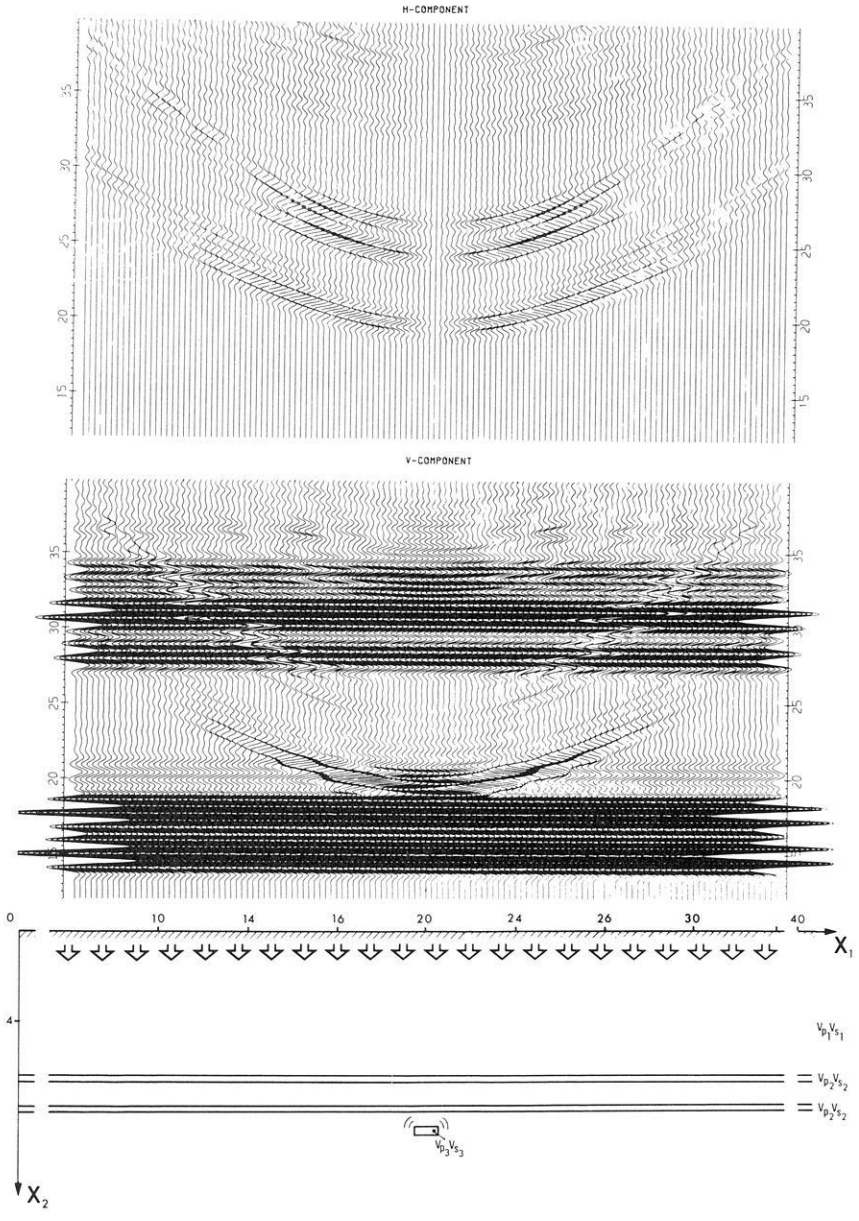

Fig. 21. Theoretical seismograms of the vertical and horizontal components for a *P*-plane wave normally incident on a layered medium containing an inclusion with the velocity $V_{P_3}=2V_{P_1}$, $V_{S_3}=2V_{S_1}$, $V_{S_3}/V_{P_3}=0.6$. The velocities of the thin layers are $V_{P_2}=1.5\,V_{P_1}$, $V_{S_2}=1.5\,V_{S_1}$, $(V_{S_2}/V_{P_2}=0.6)$. The thickness of the layers is 0.25 *WL*, where *WL* is the dominant *P* wavelength in medium 1

sian). In: Mathematical Methods of Interpretation of Geophysical Observations, 85–114, Novosibirsk, 1979

Martynov, V.N., Mikhailenko, B.G.: Numerical modelling of propagation of elastic waves in anisotropic inhomogeneous media for the half-space and the sphere. Geophys. J. R. Astr. Soc. **76**, 53–63, 1984

Merilees, P.E., Orszag, S.A.: The pseudospectral method; Numerical methods used in atmospheric models. II, GARP Publications Series, No. 17, 1979

Mikhailenko, B.G.: Numerical solution of Lamb's problem for inhomogeneous half-space. Mathematical Problems in Geophysics (in Russian) **4**, 273–297, 1973

Mikhailenko, B.G.: Calculation of theoretical seismograms for multi-dimensional medium models. Uslovno-korrektnye zadachi matematicheskojj fiziki v interpretacii geofizicheskikh nabljudenijj (in Russian). Izv. VC SIAN SSSR, Novosibirsk, 75–89, 1978

Mikhailenko, B.G.: The method of solution of dynamic seismic problems for two-dimensional inhomogeneous media models (in Russian). Dokl. Akad. Nauk SSSR **246**, 47–51, 1979

Mikhailenko, B.G., Korneev, V.I.: Numerical simulation of seismic fields in two-dimensional inhomogeneous media. In: Simulation of wave fields. Mathematical Problems in Geophysics (in Russian) 273–297, Novosibirsk, 1983

Mikhailenko, B.G., Korneev, V.I.: Calculation of synthetic seismograms for complex subsurface geometries by a combination of finite integral Fourier transforms and finite difference techniques. J. Geophys. **54**, 195–206, 1984

Mikhailenko, B.G.: Synthetic seismograms for complex three-dimensional geometries using an analytical-numerical algorithm. Geophys. J. R. Astr. Soc. **79**, 963–986, 1984

Nussbaumer, H.: Fast Algorithms for the computation of convolutions and DFTs. Springer Series in Information Sciences, Vol. 2. Springer, Berlin-Heidelberg-New York, 1981

Voronin, V.V.: Numerical solution of two-dimensional problems of diffracted elastic waves on the elastic body (in Russian). Report No. 123, Novosibirsk, VC SOAN SSSR, 1978

Shite, J.E.: Computed waveforms in transversely isotropic media. Geophysics **47**, No. 5, 771–883, 1982

Received November 24, 1984; revised version May 21, 1985
Accepted May 23, 1985